Characterizing rockfall hazard with an integrated kinematic analysis and runout model: Skagway, Alaska, USA

Ian D. Wachino[1], Joshua J. Roering[1], Reuben Cash[2], and Annette I. Patton[3, 4]

[1]Department of Earth Sciences, University of Oregon, Eugene, OR, 97403, USA
[2]Environmental Department, Skagway Traditional Council, Skagway, AK, 99840, USA
[3]Sitka Sound Science Center, Sitka, AK, 99835, USA
[4]College of Forestry, Oregon State University, Corvallis, OR, 97331, USA

Corresponding author: Joshua J. Roering (jroering@uoregon.edu)

Abstract

Rockfall is common in steep terrain and poses a hazard to nearby communities. While rockfall triggering mechanisms are highly variable and difficult to quantify, the susceptibility of rock slopes to planar, wedge, or toppling failure can be readily assessed using kinematic analysis. As such, valley slopes with favourable joint orientations exhibit high rockfall susceptibility although the potential for rockfall runout to impact infrastructure and public safety depends on the morphology of downslope terrain. Integrating rockfall susceptibility and runout models with maps of talus deposits accumulated from past rockfall events is an effective combination of tools to inform mitigation but can be difficult to realize across extensive areas. Here, we combine these methods with a historic rockfall inventory to assess rockfall hazard in the steep and forested postglacial valleys proximal to Skagway, AK, where recent rockfall activity has imperilled public safety, infrastructure, and tourism. Our field investigations identified two steeply dipping orthogonal joint sets that favour toppling failure along NW-facing hillslopes in the lower Skagway River valley as well as the NW-facing valleys that bound nearby Dyea Bay and Nahku Bay. We used new and existing lidar data and >300 field-derived joint orientations to inform a kinematic toppling failure model that identifies likely zones of rock toppling. The predicted source zones are positioned upslope of abundant talus slopes that we mapped from field observations and lidar analyses. Along the prominent ridgeline on the eastern margin of Skagway, we used RAMMS:Rockfall to model nearly 200,000 rockfall runout events for four scenarios that account for variations in clast size and ground cover. The runout predictions highlight distinct zones of low and high rockfall hazard along the ridgeline that result from changes in hillslope morphology set by the combined influence of joint orientations and the pattern of glacial erosion. High-hazard segments of the ridgeline exhibit distinct bedrock escarpments and slope-spanning talus slopes that result from the accumulation of rockfall activity over millennia. Our findings reveal controls on past and future rockfall activity and can be used to inform mitigative measures.

1 Introduction

In steep, rocky landscapes, the detachment and downslope movement of discrete rock fragments can occur frequently and poses a significant hazard to proximal communities and infrastructure (Hungr et al., 2014). Rockfall activity has been attributed to an array of highly disparate conditioning and triggering processes, including precipitation, frost weathering, insolation, seismic activity, and slope modification (Collins and Stock, 2016; Rosser and Massey, 2022). In Yosemite Valley, CA, for example, rockfall triggers include rainfall events, snow melt, and freeze-thaw action that can increase pressure along joints (Stock et al., 2011; Wieczorek and Jäger, 1996). Furthermore, rockfalls in Yosemite Valley may also be triggered on warm summer days by cyclic solar heating, which can propagate exfoliation fractures and lead to detachment (Collins and Stock, 2016). Despite significant progress in characterizing these and other rockfall triggering mechanisms, prediction of rockfall timing and location has limited ability to inform warning systems (Rosser and Massey, 2022). Precursory rock deformation can signal future activity (Abellán et al., 2010; Rosser et al., 2007; Royán et al., 2014), but current methods to quantify precursor deformation across extensive areas composed of steep, high-relief surfaces are limited and oftentimes rockfall occurs without prior deformation (Abellán et al., 2011). As a result, identifying rock slopes with the propensity to generate rockfall, often referred to as rockfall source areas, is a key first step in mitigating rockfall hazards.

A wide array of methods has been proposed to assess the extent to which hillslopes are prone to rockfall activity. Delineating potential source zones (e.g., Loye et al., 2009) can be accomplished from direct observation of past events, which assumes the location of past detachments coincides with the location of future rockfall activity (Luckman, 1976; Matsuoka and Sakai, 1999; Rapp, 1960; Whalley, 1984). Source zones can also be inferred from distinctive evidence such as talus slope and scree deposits that have accumulated below cliff faces (Borella et al., 2019; Frattini et al., 2008; Moore et al., 2009; Stock and Collins, 2014). Coupled assessment of rock slope morphology and the properties of potential source zones is another common approach that uses digital elevation models (DEMs) for assessing source zones over large areas (Frattini et al., 2008; Guzzetti et al., 2003; Messenzehl et al., 2017; Samodra et al., 2016), while more data-intensive and physically-based deformation models can be used for slope-scale analyses (Matasci et al., 2018). In absence of rock structure data, some studies (e.g., Guerriero et al., 2024) have applied morphologic criteria (e.g., slope and curvature thresholds) to DEMs to identify anomalous rock slope protrusions that are likely to experience rockfall events (Aksoy and Ercanoglu, 2006; Frattini et al., 2008; Guzzetti et al., 2003; Marquínez et al., 2003; Sarro et al., 2024)

Because rockfall is typically localized along bedding planes, fractures, or joints, collectively referred to as discontinuities, susceptibility can also be evaluated by determining the geometry of these planes of weakness with respect to the slope and orientation of rock slopes. Kinematic analysis identifies blocks that can experience instability according to sliding, toppling, or wedge failure criteria as determined by the geometry of rock slopes and discontinuities (Fig. 1) (Bovis and Evans, 1996; Wyllie and Mah, 2004). Combining high-resolution DEMs with rock structure data can inform kinematic analyses and

62 determine the relative likelihood of different failure modes across expansive areas (Grant et al., 2016; Kundu et al., 2023;
63 Stock and Collins, 2014). Recent applications of kinematic analysis leverage lidar or photogrammetry to extract bedrock
64 discontinuity data and test kinematic failure criteria on complex slope geometries, like overhanging rock quarries (Fanos and
65 Pradhan, 2018; Gigli et al., 2022). Increasingly, the acquisition of discontinuity data is accomplished using automated
66 analysis of point cloud data acquired from terrestrial laser scanning (TLS) (Matasci et al., 2018) or lidar or photogrammetry
67 acquired from uncrewed aerial systems (UAS) (Utlu et al., 2023). These approaches are powerful but can be challenging to
68 implement across large areas characterized by steep, rocky forested slopes where the details of rock structure are often
69 obscured by vegetation. As such, traditional, field-based means of bedrock structural characterization continue to be
70 relevant.

71
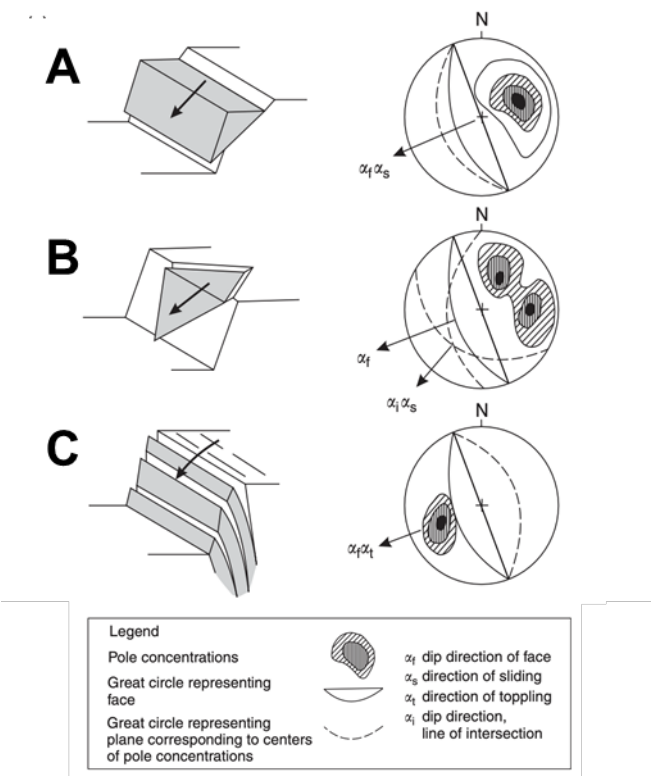
72 Figure 1. Schematic representation of common rock slope failure modes: (a) planar sliding, (b) wedge, and (c) toppling. On
73 the right of each diagram are stereonets, where the rock slope face is represented by a solid black line, and poles to planar
74 discontinuities that meet conditions for failure in shaded contours. Dashed lines represent planes of these discontinuities.
75 Modified from Wyllie and Mah (2004).

76

77 Initially, rock fragments move via creep, sliding, toppling, or falling before traveling downslope by following ballistic paths
78 and rolling across rocky or talus slopes until sufficient energy dissipation has occurred via impacts or friction (Caviezel et

79   al., 2021). Computational rockfall runout models that account for the physics of these rockfall processes can estimate the

80   trajectories and kinetic energy of falling rocks to determine potential downslope impacts (Leine et al., 2014). Many DEM-

81   based tools exist with a range of parameterization options to perform physically-based rockfall simulations and predict the

82   path of rocks over complex terrain and across variable land cover (Lu et al., 2021; Moos et al., 2021). These models have

83   been successfully employed to mitigate rockfall hazard with diversion and attenuation structures, development setbacks,

84   signage, or other means, in a variety of settings, including mines and national parks (e.g., Stock and Collins, 2014) such that

85   rockfall risk can be reduced even though accurate prediction of triggering events remains elusive.

86

87   Although rockfall activity occurs in a wide range of geologic and climatic settings, it is particularly commonplace in post-

88   glacial landscapes owing to glacial erosion that alters near-surface stresses, fracture density, topographic variations from

89   glacial erosion, and changes in environmental conditions that occur in the wake of retreating glaciers (Ballantyne, 2002;

90   Leith et al., 2014). In particular, the spatial pattern of glacial erosion can follow the fabric or trend of bedrock discontinuities

91   and set up failure-prone conditions across extensive areas. As such, relatively small changes in the orientation and geometry

92   of glacial valleys relative to the orientation of discontinuities can result in significant and systematic variations in rockfall

93   susceptibility. Although it has been implied that the cumulative impact of small but frequent rockfalls in post-glacial settings

94   can match that associated with large-scale but less frequent catastrophic or progressive rock slope failure, data are currently

95   unavailable to rigorously test this notion (Barlow et al., 2012; Corominas et al., 2014; Hales and Roering, 2007; Hungr et al.,

96   1999; Moore et al., 2009; Rosser and Massey, 2022).

97

98   Rockfall activity is common across much of Southeast Alaska but has been particularly acute in the Municipality of

99   Skagway, which is situated in a narrow, glacially carved valley herein referred to as the 'Skagway River valley, and hosts

100   vigorous cruise ship tourism from late spring to early fall. Indigenous knowledge of avalanches in the area has been

101   established (Thornton, 2010) and western documentation of rockfall activity in Skagway began in the late 1800s when gold

102   prospecting fuelled the establishment of the town. Following decades of sporadic activity, several large rockfall events in

103   summer 2022 impacted cruise docks along Skagway Harbor and generated renewed concern about the extent and scope of

104   rockfall hazards in the area. In particular, the extent and timing of past rockfall activity is not well known and the

105   susceptibility of rockfall initiation and runout in the area, and particularly along a ~5km long ridgeline that abuts the harbour,

106   town centre, and railroad, has not been characterized. In this contribution, we summarize historic and geologic data that

107   reflects the distribution and timing of past rockfall activity, document rock structure data from field observations, and

108   synthesize new and existing lidar data from airborne and UAS platforms to inform a kinematic analysis susceptibility and

109   dynamic runout model for Skagway and the surrounding area. Our findings establish the pervasive imprint of rockfall

110   activity along slopes oriented to promote toppling failure. We highlight how the pattern of glacial erosion resulted in

111   substantial rockfall erosion and cliff retreat along favourably oriented slopes while unfavourably oriented slopes experienced

112 minimal modification since glacial retreat. Our coupled modeling reveals reveal high variability in potential impacts which

113 can inform mitigation efforts.

2 Study area: Skagway, SE Alaska

115 Near the northern extent of the Alaska panhandle, Skagway is situated in the Taiya Inlet atop deltaic and fluvial deposits

116 near the outlet of a deep fjord (Fig. 2). The surrounding terrain is steep and rugged, composed of Tertiary granodiorite of the

117 Coast Range Batholith, a belt of plutonic and metamorphic rocks that extends to northern Washington (Yehle and Lemke,

118 1972). Deformation in southeastern Alaska and southwest Yukon is governed by the subduction and translation of

119 the Pacific-Yakutat plates relative to the North American plate in the St. Elias region (Biegel et al., 2024). The Eastern

120 Denali Fault and the Chatham strait fault lineaments, both strike-slip fault systems, meet just south of Skagway (Choi et al.,

121 2021). Deformation associated with these structures appears to impart a significant influence on the orientation of glacial

122 valleys, as fjords in the area tend to be linear, striking north and northeasterly (Yehle and Lemke, 1972). A dam

123 reconnaissance study focused on West Creek, a drainage just 9 km northwest of Skagway identified three joint sets in the

124 granodiorite bedrock (Fig. 3c), two abundant sets with northeast-strike and vertical or steep dips to the south, and one less

125 abundant set with northwest-strike and a consistent vertical dip (Callahan and Wayland, 1965). The authors also noted the

126 coincident orientation of topographic lineations in the area and the strike of joints interpreted to be splays from the Chatham

127 strait lineament, which is related to the nearly 3,000-km long Denali fault system. Spacing between the joints is variable,

128 ranging from 1 to 4 meters, and the joints do not exhibit slickensides or cataclastic fabric (Fig. 3a,b). Sheeting joints in

129 granodiorite observed near the tops of glaciated ridges are slightly curved or irregular, tend to parallel the ground surface,

130 and spaced from 1 to 2 meters apart at the surface.

131

132
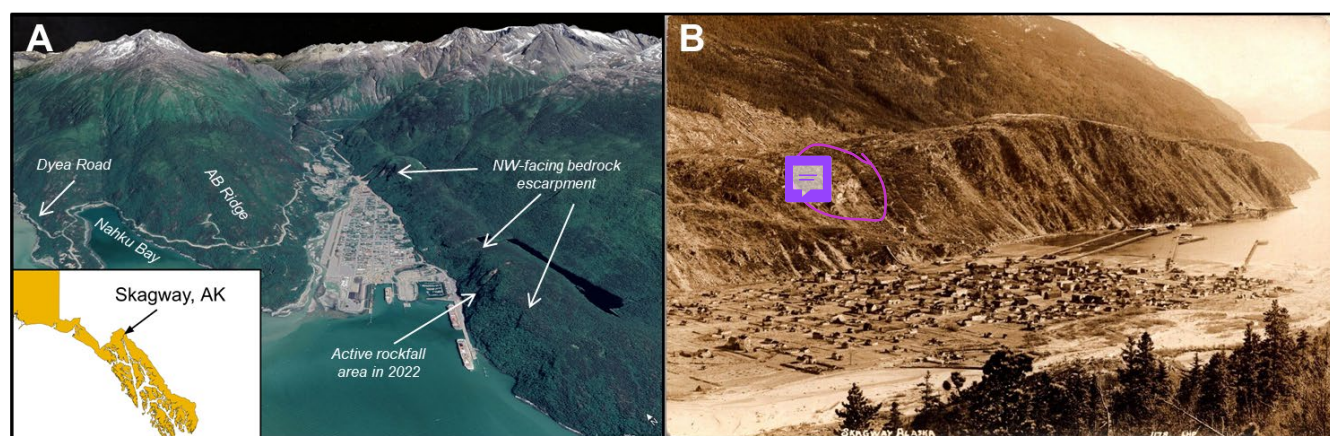
Figure 2. Study area. (a) Oblique view looking N-NE into Skagway River valley, Alaska. Note active rockfall along the NW-facing ridgeline and escarpment above the harbour and cruise ship docks. Use of Google Earth ©2025 permitted for non-commerical use. (b) Oblique view from AB Ridge looking SE across Skagway towards the NW-facing ridgeline and escarpment. This undated historic image (Wright et al., 2021) postdates the late 1890s construction of the current Skagway City Hall and Museum. Note the lack of vegetation and the sharp bedrock escarpment along the crest of the ridgline and the abundance of active talus slopes that connect to the harbour.

Regional studies of glacial history imply that the most recent episode of major glacial retreat and valley exposure in Skagway occurred 10 to 12kya (Baichtal et al., 2021; Menounos et al., 2017) and icefields persist today in nearby inland valleys. The steep slopes around Skagway are generally devoid of glacial till owing to post-retreat erosion and deposition in valley floors in the form of alluvial fans and colluvial deposits.
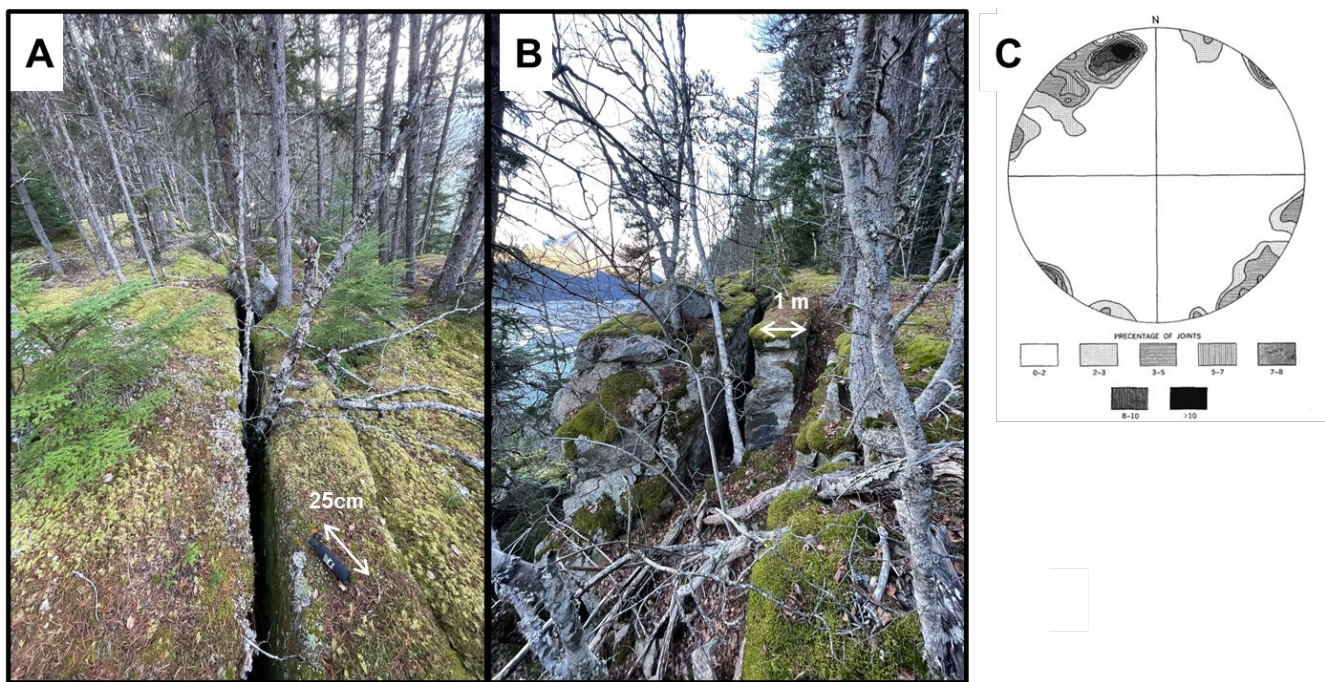
Figure 3. Images (a) and (b) of open joints and incipient toppling along the bedrock escarpment on the NW-facing ridgeline above Skagway Harbor. Equal-area, lower hemisphere stereonet with 1% area contours of 60 joints measured near Dyea, west of Skagway. Photos in a and b by Ian Madin and Josh Roering. Modified from Callahan and Wayland, 1965. See Fig. 4 for location.

Currently, Skagway experiences a subarctic maritime climate, characterized by cool summers and cold, snowy winters and current average summer temperatures range from 10 to 21°C, with occasional rainfall, and winter temperatures range from -

154 12 to -1°C, with heavy snowfall, and freezing conditions. High winds that funnel up the Taiya Inlet are common and for

155 decades it was reported that Skagway's name originated from Tlingit words describing north winds (Thornton, 2010)

156 although recent research concludes that the name derives from a contraction of 'Wushigagu Ye', which translates as "the

157 Place with Solid Core Trees" (X. Twitchell, pers. comm, 2024). Compared to other areas in SE Alaska, Skagway receives

158 low precipitation (mean annual precipitation is 1.1m) owing to the rain shadow imposed by the bounding coastal ranges to

159 the south. Atmospheric rivers account for nearly 70% of annual rainfall in Skagway and intense precipitation associated with

160 these phenomena occur with highest frequency and intensity from August to October (Nash et al., 2024). Skagway hosts a

161 coastal rainforest of spruce, pine, and cedar trees with dense underbrush at low elevations (under 1,000m above sea level)

162 and high-alpine tundra above tree line. Historical photographs and descriptions suggest that forests covering the slopes

163 perched above Skagway Harbor and township were disturbed timber through harvest and burning in the early 1900s (Wright

164 et al., 2021).

165

166 Early Western descriptions of rockfall activity in Skagway tend to focus on impacts to the harbour and railroad, including a

167 series of events in 1901 that recorded burial of the tracks near the approach to the wharf (The Daily Alaskan, 1901). The

168 location of this event coincides with the steep rocky slopes above Skagway Harbor, which have generated numerous

169 rockfalls since that account (Fig. 2). A study of geologic hazards in Skagway noted the striking linearity of N- and NE-

170 oriented fjords and valleys and identified abundant actively eroding bedrock escarpments on a NW-facing ridgeline that runs

171 along the eastern margin of Skagway that coincides with a zone of historic rockfall activity (Yehle and Lemke, 1972).

172 Downslope of these escarpments are colluvial deposits, consisting of landslide deposits, including talus from historic rockfall

173 events. The abundance and extent of these deposits implies significant slope adjustment and retreat since glacial retreat and

174 the relative activity of the deposits is based on the abundance or absence of vegetation cover. Across the valley on the

175 western side of Skagway, these talus deposits are much less prevalent, and the Yehle and Lemke (1975) maps do not indicate

176 the presence of erosional escarpments. On June 23, 2022, rocks detached from the eastern ridgeline and impacted the cruise

177 ship dock where pedestrian traffic is frequent (Munson, 2022b). Two more rockfall events originating in the rocky slopes

178 above the harbour followed in rapid succession on August 3 and 5, 2022 (Munson, 2022a).

179

180 Rockfall hazard mitigation in the area is currently focused on the active rockfall source areas above the cruise ship dock in

181 Skagway Harbor. Engineering efforts have been completed, which include wrapping rock mesh covers over source areas,

182 installing attenuator nets to block falling rocks, and scaling loose rocks (Brennan and Whistler, 2022). Instrumentation has

183 been installed to monitor the source area, including extensometers installed at the top of the slope, which show that

184 movement in the slide mass has increased from 4 cm per year to 6.5 cm per year as of 2022 (Brennan and Whistler, 2022).

185 Notably, the small section of rocky slopes above Skagway's cruise ship dock, where the engineered mitigation and

186 monitoring efforts are focused, is a small fraction of the roughly 5-km long stretch of ridgeline that borders the eastern

187 margin of Skagway. Rocky escarpments and talus deposits have been noted along the entire ridge (Yehle and Lemke, 1972),

188   including the "Cemetery Slide", a rockfall source area and runout zone stripped of vegetation by falling debris, which is

189   similar to the active source areas above the cruise ship dock. Although these zones of localized activity are well known, the

190   forest cover obscures the geologic and topographic signature of past rockfall activity along the remainder of the ridge such

191   that the pattern of relative susceptibility and runout remains ambiguous.

3 Methods

3.1. Overview

194   Motivated by renewed rockfall activity, this study seeks to identify areas susceptible to rockfall initiation and runout within

195   the steep, post-glacial valleys around Skagway. Our analysis extends to the west of Skagway along Dyea Road to the Tlingit

196   settlement of Dyea and the Chilkoot Trailhead, which is a well-travelled corridor that also provides the opportunity to test our

197   methodology across a wider range of topographic and structural configurations (Fig. 4). The components of our analysis

198   include a historical rockfall inventory, synthesis of new and existing lidar data, geomorphic and structural mapping, kinematic

199   analysis of rockfall susceptibility, and rockfall runout modelling.
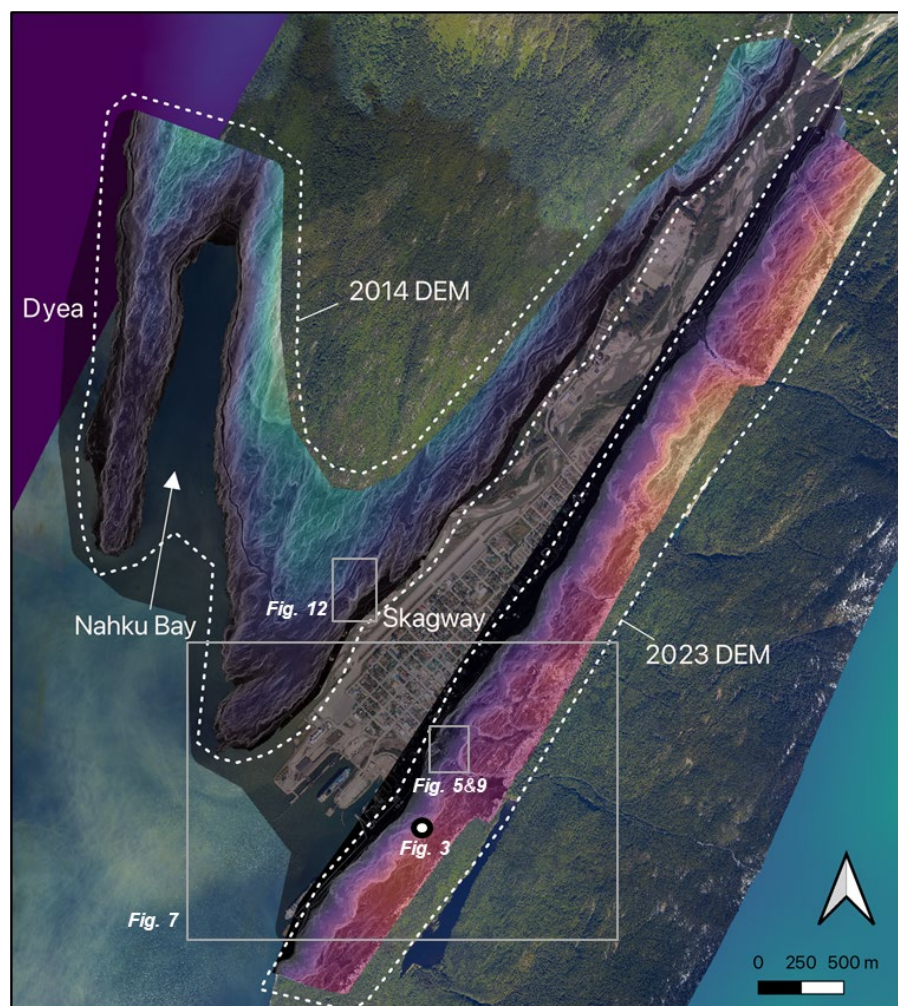
Figure 4: Location map of Skagway River valley, Nahku Bay, and Dyea showing 2014 airborne survey and 2023 UAS lidar DEM acquired for this study. The dashed lines demarcate the areas analyzed in this study. Gray boxes denote the extent of other figures. Background image from USGS NAIP (National Agriculture Imagery Program).

3.2 Rockfall inventory

We searched newspaper articles (primarily the Skagway News) and public announcements that describe the location and timing of rockfall events since August 26, 2017, which marks the beginning of rockfall mitigation efforts along the Skagway Harbor. In addition, we accessed data generated for rockfall events between 2005 and 2022 from the GeoEvent Slope Stability Database generated by the Alaska Department of Transportation & Public Facilities (AKDOT) Geotechnical Asset Management Program (Thompson, 2017). This database features details from AKDOT maintenance and operations reports,

211 including the location, date, event type (e.g., debris flows, rockfalls, landslides, snow avalanches, flooding), relative

212 magnitude, and cost, of geologic events that impact the Alaska highway system.

3.3 High-resolution topography: Airborne and UAS lidar

214 Our analysis used two sources of lidar data to inform geomorphic and bedrock mapping, kinematic analysis, and runout

215 modelling. One lidar DEM acquired in 2014 with an average ground classified point density of 4.6 m^{-2} is available from the

216 Alaska Department of Geological and Geophysical Surveys (DGGS Staff, 2013)and includes low-elevation terrain in the

217 Skagway River valley, Nahku Bay, and part of Dyea valley (Macpherson et al., 2014). Because this lidar acquisition does not

218 span a significant portion of Skagway's rockfall-prone east ridge that abuts the township and harbour, we conducted a UAS

219 lidar survey in 2023 (Fig. 4). We acquired lidar data across the 2.3 km^2 area with peak elevations of 220 m near the cruise

220 ship docks and 320 m near the northern extent of the ridgeline (Roering et al., 2025). For the acquisition, the NSF RAPID

221 facility used a Trinity F90+ fixed wing drone with a Qube 240 lidar payload to fly ~120m above ground with 90% coverage

222 overlap. The surveyed area was slightly abbreviated due to a patch of extremely steep terrain where the UAS could not be

223 flown safely at distances sufficiently close to the ground surface to acquire data. The UAS survey produced a point cloud

224 containing 650 million total points with 200 million ground classified points, giving an average ground point density of 43

225 m^{-2}. We used the ground points to create a 1 m DEM using Cloud Compare (version 2.12.3) and combined it with the 2014

226 airborne lidar data to provide a seamless coverage for our analyses (Fig. 4).

3.4 Geomorphic mapping

228 We used field observations, historic photographs, and slope thresholds and surface texture from the combined lidar DEM to

229 identify and map talus deposits that reflect the accumulation of rockfall deposits. These talus deposits include both forested

230 and exposed occurrences. To define the characteristic slope angles associated with active talus slopes we measured slope

231 angles from 20° to 45° that coincide with mapped talus deposits along the eastern ridge. Slopes steeper than 45° tend to

232 correspond with bedrock cliffs and outcrops, whereas slopes gentler than 20° often reflect relatively uneroded bedrock

233 surfaces or deposits from fluvial or mass wasting processes. The relatively smooth texture of accumulated rockfall deposits

234 identified with hillshade and slopeshade layers (Burns and Madin, 2009) was also used to identify active talus slopes as well

235 as bedrock cliffs or outcrops that constitute a rockfall source area. Talus deposits occur on a wide range of scales and for this

236 analysis we focused on mapping patches of talus with area >100m^2 to ensure accuracy and highlight zones of significant

237 activity (Fig. 5).

238
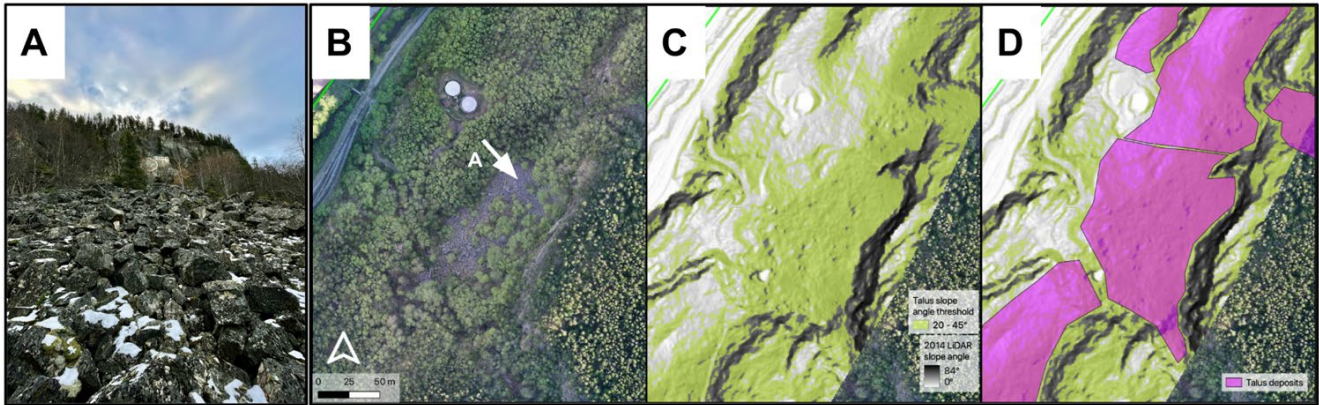
Figure 5: Field images and lidar mapping of talus mantled slopes. See Fig. 4 for location. (a) View looking SE along an exposed talus deposit with boulder sized clasts at the base of a 40 m cliff known as Kirmse's Cliff on far left of image, (b) Aerial imagery from 2023 UAS survey showing the talus deposit and cliff (center left), white arrow represents photograph location and view direction, (c) Terrain within the slope angle range of 20°-45° colored in yellow, and (d) map of talus polygons generated from lidar slope shade and slope angle maps and orthoimagery. Hillshades in c and d derived from DGGS lidar data. Background image from USGS NAIP (National Agriculture Imagery Program).

3.5 Bedrock structure and discontinuities

To quantify the geometry of joints and discontinuities that contribute to rockfall initiation, we collected structural measurements at a range of distinct locations within the study area and combined them to generate a comprehensive discontinuity dataset (Kundu et al., 2023). The steep, forested, and uneven terrain surrounding Skagway limits access to outcrops and the traditional 'scanline' method (Priest and Hudson, 1981) was untenable. Furthermore, the significant forest cover and expansiveness of the study area precluded the use of ground-based laser or SfM (structure from motion) methods for acquiring structural information. Instead, we traversed the base of outcrops as an approximation of scanlines and measured the orientation of planar surfaces expressed in the outcrop with FieldMoveClino, a digital compass-clinometer smartphone app (Oliinyk et al., 2020), which enabled rapid and accurate data acquisition. Our measurements were acquired across a wide range of locations in the study area in order to characterize spatial variations in discontinuity orientations. In particular, we visited outcrops along the eastern and western sides of the Skagway River valley as well as outcrops in secondary valleys perpendicular to these ridgelines to ensure that the full range of relevant joint orientations were represented (Terzaghi, 1965).

3.6 Kinematic analysis of rockfall susceptibility

To assess the spatial pattern of rockfall susceptibility across the study area, we adopted a kinematic analysis approach and applied criteria for planar sliding and toppling failure within our combined lidar DEM. This approach foregoes the

263 mechanical complexity and extensive parameterization of more sophisticated analyses (e.g., Matasci et al., 2018) in order to
264 generate results that span an extensive area. As described below, the remarkable consistency of discontinuity orientations
265 across the study area inspired this approach and therefore we invoked the entire distribution of measured joint orientations at
266 all locations to perform the kinematic analysis. Specifically, we applied the stability criteria for each failure mode at each
267 pixel in the combined lidar DEM by estimating the fraction of the 337 joint orientations that are predicted to be unstable
268 given the topographic aspect and slope angle of that pixel. The failure criteria for planar and toppling failure are defined
269 following Wyllie & Mah (2004) and described below. Essentially, this approach is equivalent to locally performing a
270 stereonet analysis of rock slope failure across our study area and aggregating the results to identify potential rockfall failure
271 modes as well as areas of high relative susceptibility. For the analysis, we used a friction angle of 40°, consistent with
272 measured values for jointed granodiorite similar to Skagway's lithology (Alejano et al., 2019). For validation of our
273 modelled rockfall susceptibility maps, we compared our predictions to the location of recent rockfall events in Skagway, as
274 well as mapped talus deposits which serve as a proxy for prior rockfall activity (Loye et al., 2009; Stock and Collins, 2014).
275
276 Planar slides occur when the inclination of a bedrock slab exceeds the friction angle and it slides along a planar
277 discontinuity. Toppling failures occur when discontinuities steeply dipping into the rock slope face form slabs or columns of
278 rock that rotate forward along a fixed base (Fig. 1). Two types of toppling failures can occur that are influenced by the
279 strength of the rock mass and the geometry of discontinuities. Flexural toppling, where slabs of rock bend forward until they
280 break in flexure, is typical in shale and slate where orthogonal jointing is not well developed. Block toppling is common in
281 bedrock with orthogonal joint sets, where two steeply dipping joint sets form the sides of blocks, and a third set of low angle,
282 widely spaced joints form a basal failure plane. The active rockfall source area situated above Skagway's cruise ship dock
283 has been described as a progressive toppling failure with a stair-stepped basal feature (Brennan and Whistler, 2022). Topple
284 failures observed in the field are consistent with this description, which is described by the block toppling failure
285 mechanism. As a result, our analysis focuses on block toppling although we also account for planar sliding given that
286 sporadic sliding was observed in the field. Field observations and geotechnical reports do not identify wedge failure as a
287 potential mechanism and we opted not to include it in our analyses.
288
289 The criteria for planar, wedge, or toppling failure is based on the orientation of discontinuities and their orientation relative
290 to the rock slope face (Wyllie and Mah, 2004). The dip direction of the discontinuity and rock slope is given by α_A and α_f,
291 respectively, and the dip angle of the discontinuity and rock slope, both relative to horizontal, is given by ψ_A and ψ_f,
292 respectively. The friction angle of the joint interfaces is given by ϕ.
293
294 Accordingly, a rock slope is susceptible to planar sliding failure along a discontinuity if the following three conditions are
295 simultaneously met:

296 $$|\alpha_A - \alpha_f| < 20° \; ; \; \psi_A < \psi_f \; ; \; \psi_A > \phi \qquad (1)$$

297 The first condition requires that the interfaces are aligned in a sufficiently similar orientation (in this case within 20°) while

298 the second ensures that the discontinuity dip is shallower than the angle of the bedrock slope such that the discontinuity

299 intersects or 'daylights'. The third and final condition demands that the interface slope angle exceeds the angle of friction. All

300 three conditions must be met at a given location for planar sliding to be deemed likely.

301

302 For block toppling failure, the following two conditions must be met simultaneously:

303 $$\alpha_f - 20° < (\alpha_A \pm 180°) < \alpha_f + 20° \; ; \; (90° - \psi_f) + \phi < \psi_A \qquad (2)$$

304 The first condition asserts that the discontinuity must dip into the rock slope face and be parallel, or nearly parallel (e.g., within

305 20°), to the dip direction of the slope face. The second condition indicates that the discontinuity dip must exceed the friction

306 angle allowing for interlayer slip between the blocks. In our model, the maximum allowable dip direction deviation is ± 20°

307 for both planar slide and block toppling failure. Although this value was often chosen to be ± 10° for block toppling we

308 expanded the constraint to ± 20°, consistent with recent contributions (Cruden, 1989; Gigli et al., 2022).

309

310 Kinematic analysis requires discontinuity data that is locally representative. Traditionally, discontinuity measurements are

311 taken in the field, whereas many modern applications extract discontinuity orientations from high-resolution point clouds of

312 the rock slope face (Utlu et al., 2023). Field measurements remain a reliable and relevant means to capture joint orientations

313 (Kundu et al., 2023), especially in locales where terrestrial laser scans are not feasible due to hazardous terrain or where

314 slope faces are obscured by vegetation.

315

316 Using equations 1 and 2, we estimated the number of joints in our field-derived dataset (n=337) that are predicted to exhibit

317 planar and toppling failure, respectively, for each pixel in our combined lidar DEM. Our maps of planar and toppling failure

318 are then calculated as the percentage of joints that meet the conditions required for failure conditions. For example, a

319 toppling failure index value of 0.31 for a given pixel in our DEM indicates that 31% of the joints in our joint dataset satisfy

320 the two conditions in equation 2. This approach provides a description of relative rockfall initiation susceptibility across our

321 study area.

322 **3.7 Rockfall runout modelling with RAMMS**

323 To model potential runout paths associated with rock slopes that have high rockfall susceptibility, as determined by our

324 kinematic analyses, we used the 3D rockfall simulation software RAMMS:Rockfall (https://ramms.ch/ramms-rockfall/) to

325 represent the sliding, bouncing, and rolling motion of rock clasts. This model accounts for the energy balance of falling rocks

326 and has been used extensively at a range of scales for both applied and fundamental research studies (Leine et al., 2014; Lu

327 et al., 2019). The primary inputs required for the RAMMS model include digital elevation data (i.e., DEM), the location of

328 rockfall source areas, specification of ground cover, and the shape and size of the falling blocks.

329

330 We used our combined lidar DEM, which has a 1x1 m pixels and spans the area shown in Fig. 4. To identify potential source

331 areas, we identified pixels in our maps of toppling susceptibility with values greater than 5%. Pixels with >5% toppling

332 susceptibility demarcate rocky cliffs situated above our mapped talus deposits as well as areas of recent rockfall activity in

333 the Skagway Harbor (Fig. 5). The pixels with a >5% high toppling susceptibility were converted to polygons and only

334 polygons with area greater than 25 m^2 were retained in order to eliminate local high-relief features like boulders and trees

335 that can perpetrate the signature of rockfall source zones. Rockfall source points for RAMMS modelling were randomly

336 distributed across the polygons with a density of 0.02 m^{-2} and a minimum point spacing of 5 m. This methodology follows

337 convention used in other studies (Lu et al., 2021) and yielded nearly 5,000 rockfall initiation points for our RAMMS

338 simulations.

339

340 The slopes east of Skagway are heavily forested, except in locations where falling debris has stripped vegetation, such as the

341 cruise ship dock and at the northern extent of the eastern ridge bordering Skagway. In RAMMS, we represented forested

342 areas as spruce alpine forests and trees were simulated in these areas using the 'dense forest' category in RAMMS, which is

343 defined by a stem density of 600 trees per hectare with a mean diameter of 30 cm. These parameters were chosen based on

344 our field observations and the typical density of mixed red alder coniferous stands in Southeast Alaska (Poage et al., 2007).

345 The effect of trees in the RAMMS rockfall runout module is to attenuate energy and reduce velocity, thus constituting a

346 significant impact on hazard potential. The very small amount of terrain (less than 5% of the study area) that exists outside

347 these forested areas was set to the fine talus category in RAMMS, which reflects negligible ground cover atop relatively

348 fine-grained talus deposits. We performed simulations with and without forest cover in order to assess the potential role of

349 timber harvest and fire on rockfall runout and provide a conservative assessment of the hazard extent.

350

351 We estimated representative block size and shape by measuring blocks in exposed talus piles. To estimate block size, the

352 intermediate axis of 74 blocks was measured from high-resolution point clouds combined with orthoimagery. We determined

353 the mean intermediate axis size to be 1.08 m while the 50th percentile was 0.66 m and the 95th percentile was 3.56 m. Blocks

354 observed in the field are typically tabular and the shape of blocks was estimated by measuring the long, intermediate, and

355 short axes of 10 blocks with sufficient exposure to allow measurement using our UAS-derived point clouds. The block

356 dimensions were measured and we applied the resulting aspect ratio to the 50th percentile and 95th percentile intermediate

357 axis values from our block size measurements. The dimensions of the resulting rocks used in the simulation were 0.94 m x

358 0.66 m x 0.37 m (medium, 50th percentile), and 5.10 m x 3.56 m x 1.99 m (large, 95th percentile), which represent moderate

359   and large clast sizes, respectively. Given the tendency for large clasts to travel longer distances, our 95th percentile blocks are

360   intended to reflect the conservative (or long runout) scenario.

361

362   To simulate the range of potential rockfall impacts, we focused on four scenarios for RAMMS simulation with the following

363   parameterizations: 1) 50th percentile clasts with no forest cover, 2) 50th percentile clasts with dense forest, 3) 95th percentile

364   clasts with no forest over, and 4) 50th percentile clasts with dense forest. To account for the stochastic nature of rockfall

365   release, we used RAMMS to select 1 of 10 randomly chosen rock clast orientations to be released at each source point,

366   yielding nearly 50,000 individual rockfall runout paths in each of the four simulations.

367

368   For our runout analysis, we focused on the eastern NW-facing ridgeline of the Skagway River valley given the need to assess

369   impacts to the harbour and township. Because each simulated runout event results in an individual rockfall path, it can be

370   difficult to effectively visualize the cumulative pattern of predicted runout. To identify terrain with high likelihood of

371   rockfall runout we used RAMMS to count the number of rockfall events that traversed each pixel in our domain for each of

372   the four scenarios. As such, the cumulative number of rockfall passages at each pixel accounts for both the abundance of

373   upslope source areas as well as the tendency for topography to steer or direct rockfall into particular pathways. In addition,

374   we used RAMMS to create a "digital" boundary (or barrier) coincident with the railroad tracks along the base of the

375   ridgeline to record the number and kinetic energy of modelled rockfalls that bypass the boundary and impact the harbour and

376   township.

377   **4 Results**

378   **4.1 Rockfall inventory**

379   Descriptions of rockfall events before 2005 can be found in newspaper articles dating back over a century, although we focus

380   on recent events in this contribution. We identified 11 reported rockfall events reported in the Skagway News since 2017

381   (Table 1). These reports tended to reflect sporadic rockfalls along Dyea Road as well as activity in 2022 abutting Skagway

382   Harbor on the eastern ridgeline. Many reports are recorded in the police blotter section of the Skagway News, but the timing

383   and location of these events is sometimes unclear and those cases were not included in our rockfall inventory. The AKDOT

384   GeoEvent database includes 536 reports of rockfall-related maintenance and operation activities in our study area between

385   2005 and 2022. Notably, this database does not include events along the eastern ridgeline in Skagway because those events

386   do not impact the state highway system. Rather, the vast majority (>415) of the AKDOT reports originate from the NW-

387   facing sections of Dyea Road west of Skagway. Among those events, 7 resulted in road closures that lasted 3 days or longer

388   in March 2012, October 2012, January 2014, March 2015, February 2016, September 2016, and December 2020.

389

390   Table 1: Rockfall events reported in the Skagway News since 2017

Event date	Event time (local)	Pre-event 24-hr rainfall total (inches)	Location
9-Oct-2023	n/a	0.63	East Dyea Valley
7-Oct-2023	n/a	1.46	Eas Nahku Bay
18-May-2023	6:17pm	0	North Slide
29-Sept-2022	3:57pm	0.50	East Nahku Bay
5-Aug-2022	n/a	0.04	North Slide
3-Aug-2022	5:00pm	0.02	North Slide
23-Jun-2022	7:30am	Trace	South Slide
2-Dec-2020	12:23pm	3.24	East Nahku Bay
5-Sept-2017	5:30am	0.76	North Slide
5-Sept-2017	3:00am	1.05	North Slide
26-Aug-2017	6:30am	0.55	North Slide

391

392 Rockfall events reported in the newspaper and AKDOT database occur sporadically throughout the year with most activity

393 in the summer and fall months. Some high impact events correspond with intense rainfall events although most events do not

394 coincide with an obvious climatic trigger. Rockfall activity on December 2, 2020, was preceded by over 3 inches of rainfall

395 in the previous 24 hours. By contrast, a May 2023 event, which we observed in the field, initiated on a clear, sunny day with

396 no precipitation in the 24 hours leading up to the event. In addition, the August 2022 events that impacted Skagway Harbor

397 were not preceded by notable rainfall. Thus, while precipitation plays a role in initiating some rockfall events in Skagway

398 other triggers maybe relevant making prediction difficult.

399 **4.2 Geomorphic mapping**

400 The morphology of glaciated valleys around Skagway is variable owing to bedrock structure, differential glacial erosion, and

401 post-glacial landscape evolution. These factors generate systematic variations in the abundance of bedrock cliffs that serve as

402 rockfall source areas as well as long, steep slopes that facilitate long rockfall runout. On the east side of the lower Skagway

403 River valley, our lidar DEM and field observations reveal a distinct northwest-facing bedrock escarpment that runs parallel

404 just below the crest of the ridgeline (Fig. 1, 6). This feature is particularly distinct above the cruise ship dock, where the

405 ridgeline has high relief compared with sections to the north that abut the township. A similar high-relief escarpment also

406 emerges on the same ridgeline near the northern extent of the township. Below these bedrock escarpments, we observe

407 abundant talus deposits that extend continuously downslope to the base of the ridgeline and the valley floor (Fig. 6). An

408 undated historic photograph which postdates the 1899 construction of the current Museum and City Hall depicts the eastern

409 ridgeline in a state of minimal forest cover such that the escarpment and talus slopes above the harbour are clearly visible

410 (Fig. 2b). These observations imply substantial post-glacial erosion through lateral (southeastward) retreat of the ridgeline as

411 talus slopes convey bedrock downslope creating long and relatively smooth pathways for rockfall runout. On that image, the

412 ridgeline slopes just north (on the left side of the image) exhibit gentler slope angles and a benchy morphology which

413 implies less extensive post-glacial erosion and slope modification via rockfalls (Fig. 2b). Atop the ridgeline and east of the

414 escarpment, the ridgeline contains abundant evidence of unmodified glacial erosion features. The west side of the lower

415 Skagway River valley has a very different morphology, in that it lacks a distinct escarpment and instead exhibits consistent

416 and gradual slopes that imply minimal post-glacial modification. Locally, we observe vertical cliffs along the Skagway

417 River. Otherwise, the topography on the west side of the lower Skagway River valley primarily consists of rock slopes that

418 form prominent ridges that parallel the strike of the valley. We observe a similar pattern of bedrock escarpments and talus

419 deposits along northwest-facing slopes of two parallel ridgelines between Skagway and Dyea (Fig. 6).

420

421

422
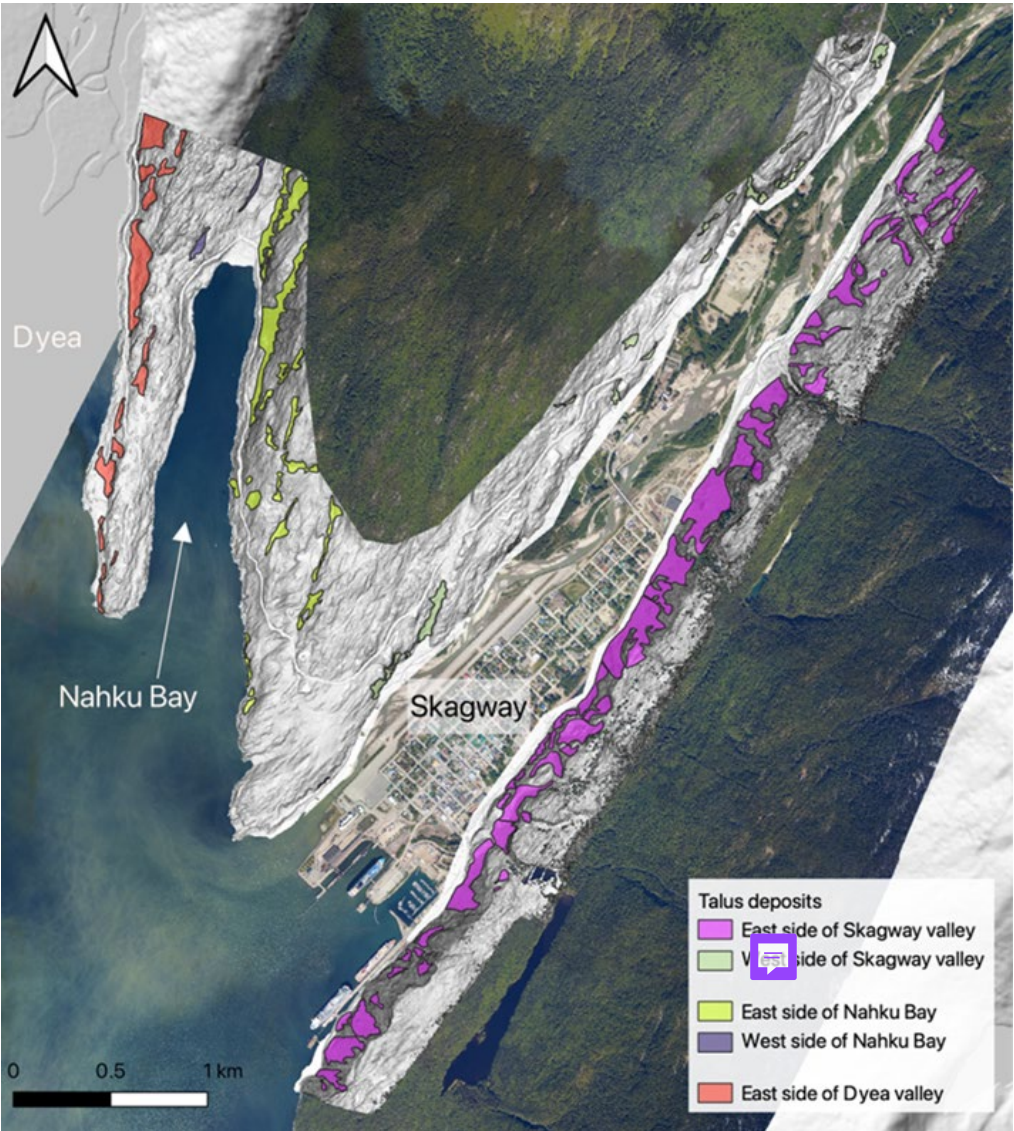
423 Figure 6: Distribution of talus deposits in study area. Polygons identified by their location: Skagway River valley, Nahku Bay,
424 and Dyea valley. Note the abundance of talus deposits on the NW-facing ridgeline in Skagway and on NW-facing slopes in

425   Nahku Bay and near Dyea. Hillshade derived from DGGS lidar data. Background image from USGS NAIP (National
426   Agriculture Imagery Program).

427

428   Our lidar- and field-derived mapping revealed abundant talus slopes on northwest-facing ridgelines across our study area.
429   More generally, talus deposits compose 12% of the 7.2 km² total mapped area. Along the eastern ridgeline, we identified 56
430   talus slopes with an average area of 9,290 m², which collectively make up 20% of that ridgeline area. On the west side of the
431   lower Skagway River valley, the southeast-facing ridgeline hosts 20 talus deposits, and these talus slopes constitute only 3%
432   of the 1.67 km² mapped area on that side of the valley. Similarly, talus deposits on the southeast-facing ridgelines bordering
433   Nahku Bay are much less abundant (1%) and smaller in area than on the northwest-facing ridgeline that abuts the bay (11%).

434   **4.3 Bedrock structure and discontinuities**

435   To characterize the geometry of discontinuities with the potential to generate rockfalls, we collected 337 joint orientations
436   from 36 granodiorite outcrops across the study area (Supplemental material) and plotted the data as poles to planes on an
437   equal area stereonet to identify dense clusters of poles which were then grouped into joint sets (Fig. 7). Three joint sets were
438   identified in this survey, two steeply dipping orthogonal sets (*J1 & J2*), and one set that dips gently to the west (*J3*). The
439   steeply dipping joints are of relevance, as they tend to be conducive to toppling, which is the most observed failure mode in
440   Skagway. The most densely defined joint set is J1, which parallels the strike of the lower Skagway River valley and the
441   eastern ridgeline and predominantly dips to the southeast. The less densely defined joint set (*J2*), is approximately
442   orthogonal to *J1*, has near vertical dips, and strikes northwest. The third, gently dipping joint set (*J3*), are interpreted as
443   sheeting joints, typical in plutonic rocks, which have significantly higher curvature at the outcrop scale than the steeply
444   dipping orthogonal joints resulting in an elongate field of poles on the stereonet.

445
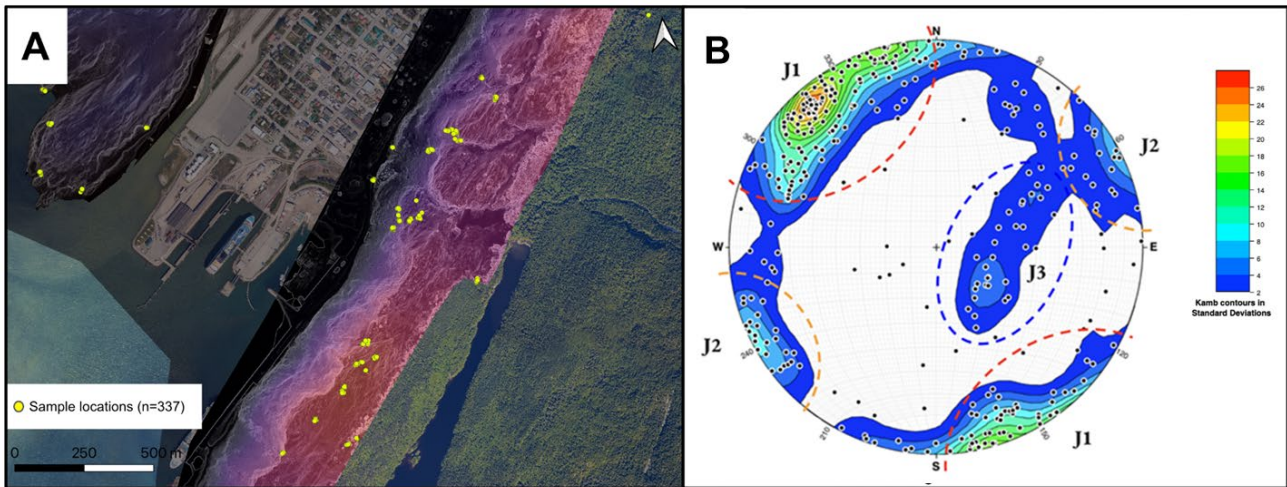
Figure 7: Structural data (a) Location of 337 structural measurements from 36 outcrop locations distributed across Skagway Valley and the AB ridgeline separating Skagway from Nahku Bay. See Fig. 4 for location. (b) Lower hemisphere equal area stereonet of joint measurements visualized as poles to planes (n=337) with Kamb contours to highlight dense clusters of poles, which were grouped into three joint sets (J1, J2, and J3). Background image in (a) from USGS NAIP (National Agriculture Imagery Program).

4.4 Kinematic analysis of rockfall susceptibility

The abundance of consistently oriented joints with vertical or sub-vertical dips suggests that rock toppling is the dominant rockfall mechanism in Skagway, which is supported by field observations. Furthermore, given the consistent orientation of sub-vertical joints, the primary control on susceptibility to toppling is the orientation and inclination of rock faces (equation 2). On the crest of the eastern ridgeline in the lower Skagway River valley, for example, the glacially flattened bench at the top of the slope is not steep enough to meet topographic conditions for either failure mode (Fig. 5). As one moves to the west side of the crest, however, the gentle ridgetop abruptly transitions to the steep escarpment where overhanging, cliffy bedrock slopes are observed. At this position on the ridgeline, our analyses show that large patches of terrain have a substantial portion (> 25%) of discontinuities that promote toppling failure according to equation 2 (Fig. 8). At downslope locations (i.e., between the ridgeline and valley floor), rock slopes continue to exhibit patchy zones of toppling susceptibility, many of which are in close proximity to Skagway township and harbour. Along the rock slopes on the west side of Skagway, our analyses reveal fewer and smaller patches of terrain susceptible to toppling with less than 10% of the discontinuities predicted to be unstable. We observe a similar pattern along the sub-parallel ridges west of Skagway along Dyea Road with northwest-facing ridgelines exhibiting abundant patches of terrain with high propensity for toppling failure (Fig. 8). Finally, we observe small areas of terrain with planar failure susceptibility according to equation 1 and in these patches, less than 5%

469   of the joints are predicted to promote planar sliding. More generally, by combining our talus slope maps with toppling failure

470   susceptible zones, we note a strong correspondence such that zones with >5% toppling failure commonly occur just upslope

471   of talus-mantled slopes (Fig. 9).

472
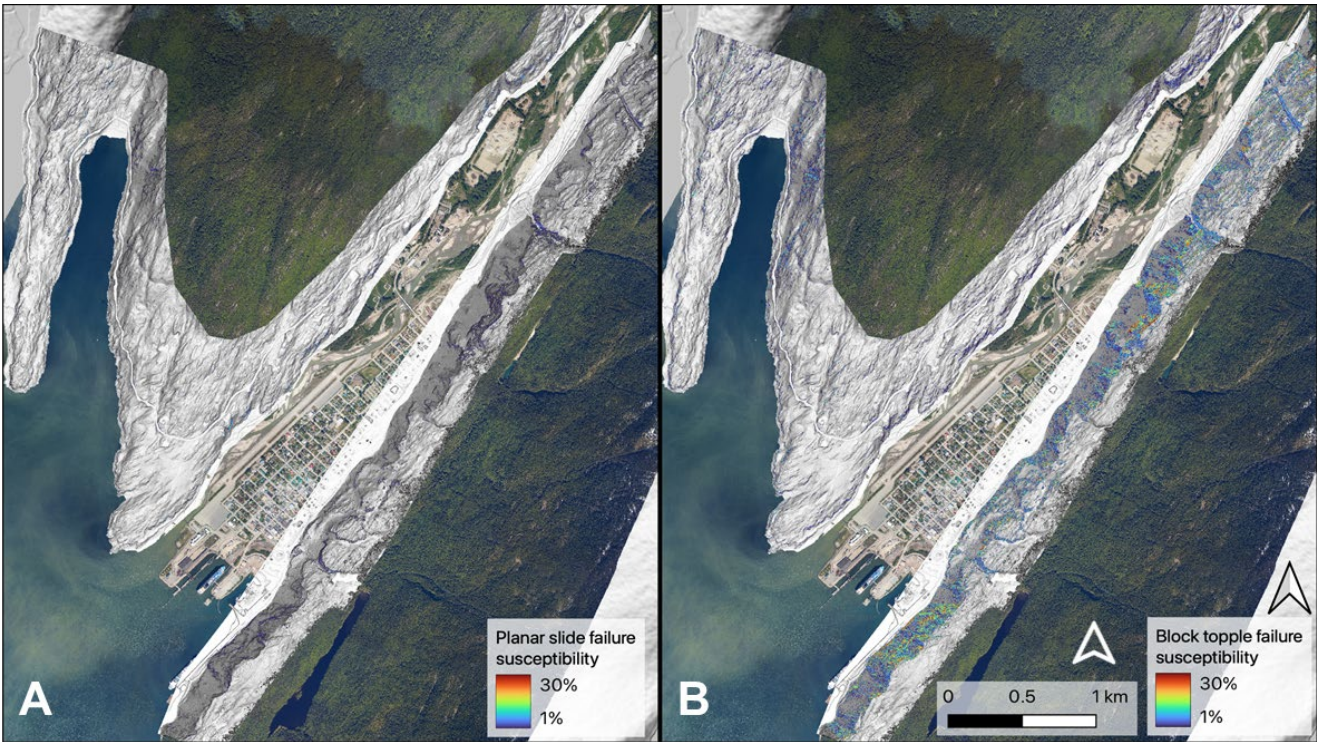
473   Figure 8: Maps of rockfall susceptibility indices using combined 2014 airborne and 2023 UAS lidar datasets. (a) Susceptibility
474   to planar slide failure according to equation 1, and (b) susceptibility to block toppling according to equation 2. Both indices
475   are estimated as the percentage of joints deemed unstable at each pixel. Note the abundance of toppling failure zones on NW-
476   facing rock slopes that border Skagway and Nahku Bay. Hillshades in a and b derived from DGGS lidar data. Background
477   image from USGS NAIP (National Agriculture Imagery Program).

478

479

480
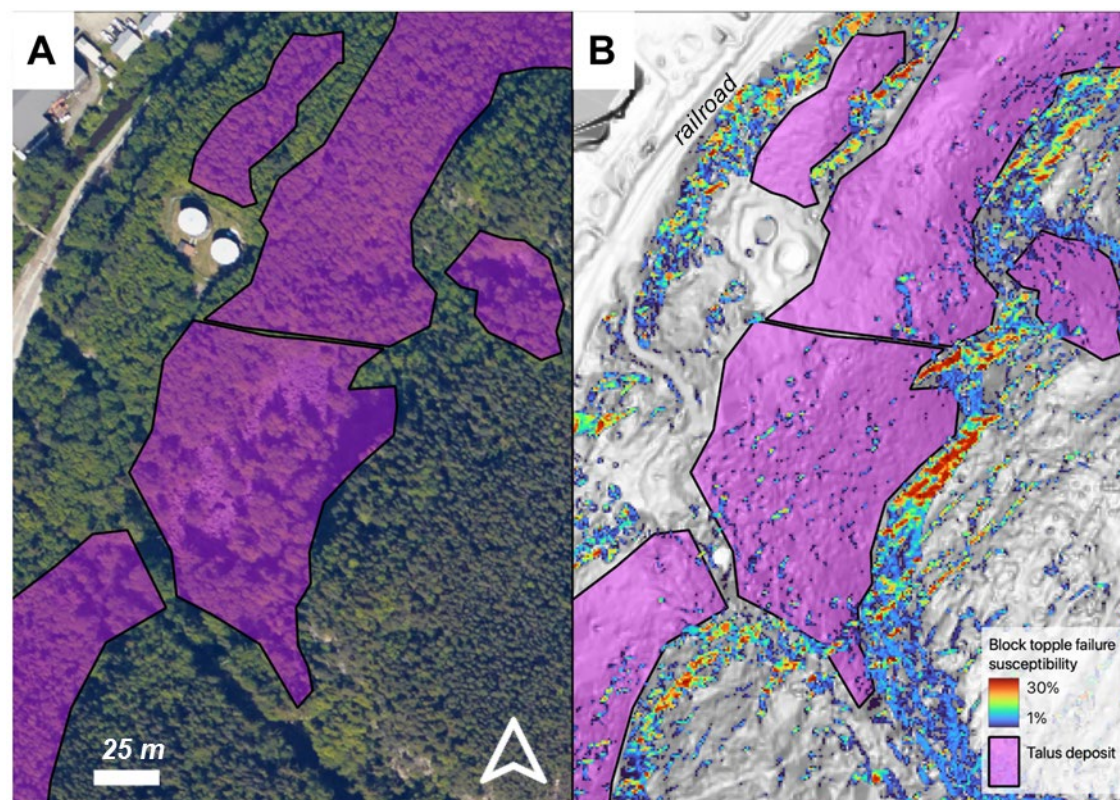
Figure 9: Map of talus deposits and block toppling susceptibility index (percentage of joints deemed unstable in each pixel according to equation 2). See Fig. 4 for location. (a) Orthoimage of Kirmse's cliff and the partially forested talus deposit at the base of the slope, (b) Block toppling susceptibility index. Note the abundance of susceptible toppling areas perched above the talus deposits. Background image in (a) from USGS NAIP (National Agriculture Imagery Program). Hillshade in (b) derived from DGGS lidar data.

4.5 Rockfall runout modelling using RAMMS

By using zones of high toppling susceptibility (>5%) as source areas for rockfall initiation we used RAMMS to model the

runout of nearly 50,000 rockfall events for each of the four scenarios that account for differences in clast size and ground

cover. Our simulations showing the total number of rockfall events traversing each pixel reveal distinct zones subject to high

rockfall susceptibility as well as extensive downslope transport (Fig. 10). In each of the four scenarios, the southern end of

the ridgeline above the harbour (between 4 and 5km on our railroad-based transect) exhibits ~10 specific chutes or paths of

likely rockfall runout whereby initiation near the escarpment results in the concentration of rockfall runout along these paths

and conveyance to the cruise ship docks and/or harbour (Fig. 10). This zone coincides with the area of high-relief terrain and

extensive escarpment development. In contrast, the central portion of the ridgeline (between 2.8 and 4km) immediately

(cc) BY

496 adjacent to much of the township exhibits patchy and less frequent rockfall activity along gentle and irregularly oriented

497 bedrock steps and benches. Further north, our simulations again reveal abundant long rockfall runout paths at the northern

498 extent of the township with a concentration near the Cemetery Slide area (between 1 and 2km). Finally, at the northernmost

499 extent of our simulation domain (near 1km), the results show patchy and short rockfall transport paths coincident with

500 gentle, benchy topography. Although the relative pattern of predicted runout described here is consistent across the four

501 scenarios, our simulations of 95th percentile size clasts and no forest cover result in the most abundant passage of rockfall

502 events to the valley floor with high potential for impacting infrastructure and imperilling public safety (Fig. 10d).

503
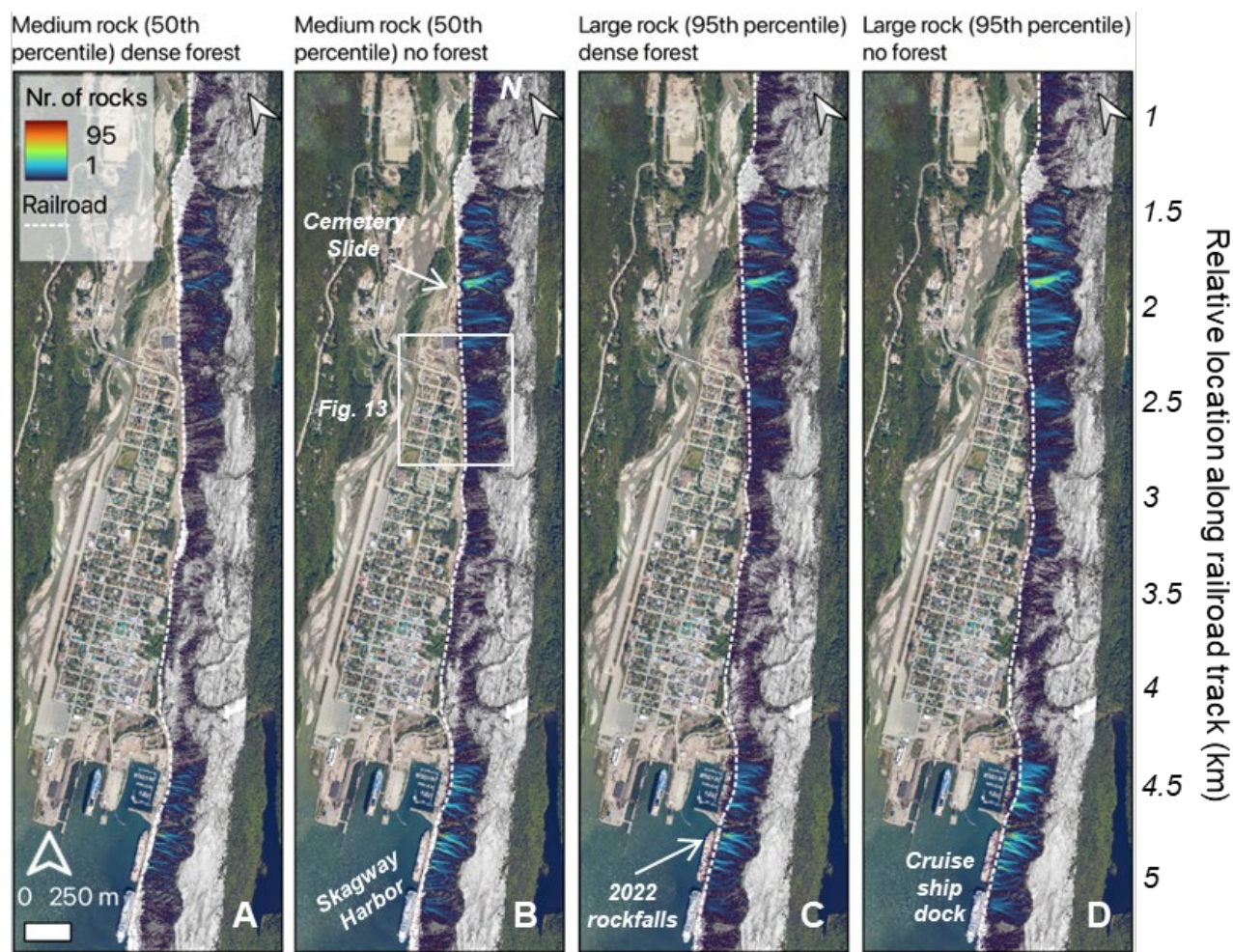
Figure 10: Map of modeled rockfall runout along eastern ridgeline in Skagway Valley conducted for 4 scenarios with variable
clast size and land cover (panels a-d). The number of rockfall events that traverse each cell is indicated by the color ramp with
warm colors reflecting frequent rockfall passage. Note the abundance of long runout events in the SW section bordering the
harbour and near the northern extent of the township. The dashed white line denotes the railroad track used to document
rockfall runout and kinetic energy in Fig. 11 for relative position along the tracks. The white box in (c) denotes the area shown

510 in Fig. 13, site of an historic rockfall event that impacted the township. Hillshade derived from DGGS lidar data. Background
511 image from USGS NAIP (National Agriculture Imagery Program).

512

513 To characterize the location and potential impact of simulated rockfall events that reach the valley floor, we tallied the
514 number and kinetic energy of simulated rockfall events that traverse the railroad track (Fig. 11). In each of these scenarios,
515 the north-to-south alternating pattern of high-low rockfall runout hazard is reflected in the number and kinetic energy of
516 clasts that travel to the base of the ridgeline. Given the 49,450 simulated rockfall events in each of the four scenarios, <2%
517 and 12% rocks crossed the railroad for the dense forest and no forest scenarios with the 50th percentile clast size,
518 respectively. By contrast, using the 95th percentile clast size resulted in nearly 20% and 28% rockfall passage of the railroad
519 in the dense forest and no forest scenarios, respectively. These results highlight the importance of dense forest and clast size
520 in determining risk of rockfall runout.

521

522
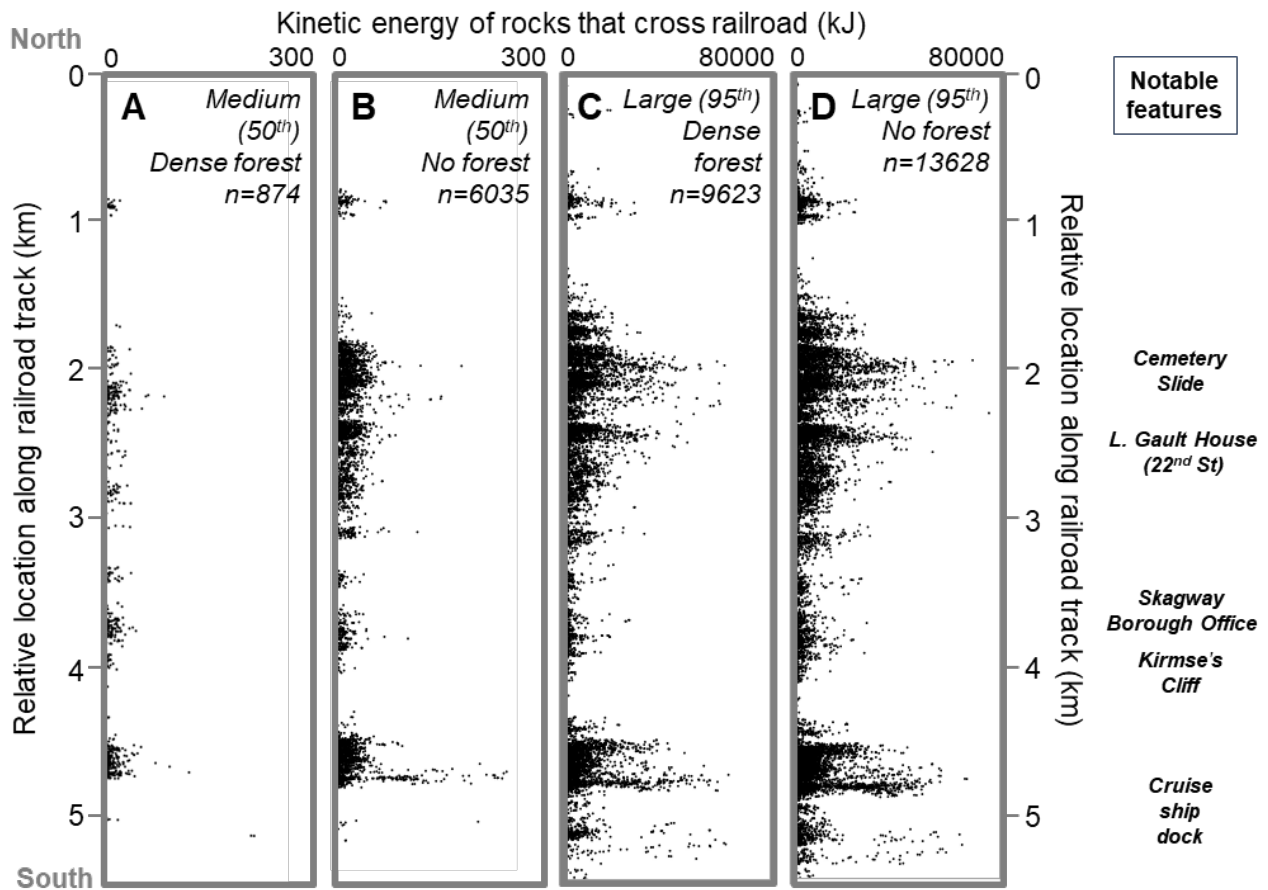
523 Figure 11: Kinetic energy of simulated rocks that pass the railroad tracks (see Fig. 10 for location) for 4 scenarios with variable
524 clast size and land cover (panels a-d). Note the difference in scale of kinetic energy between panels (a,b) and (c,d). The number
525 of rocks that pass across the track is highest for the scenario with the largest clast size and no forest cover. Notable locations
526 are annotated along the right margin of the plots.

527

528 **5 Discussion**

529 Rainfall appears to be responsible for triggering some rockfall events in Skagway, but the majority of rockfall events are not

530 preceded by heavy precipitation. Therefore, accurately predicting the timing of rockfall events based on precipitation

531 metrics, like rainfall initiation thresholds used to estimate the likelihood of landslide initiation in Sitka, AK (Patton et al.,

532 2023), is not likely to be successful. Instead, estimating the spatial pattern of rockfall susceptibility is a useful approach to

533 mitigating rockfall hazard. Taken together, our analyses of rockfall susceptibility and talus deposition maps demonstrate that

534 rockfall source areas and runout paths tend to be located on northwest-facing rock slopes in the lower Skagway River valley,

535 Nahku Bay, and the lower Taiya River valley, indicating a strong topographic control on rockfall activity owing to the

536 regularity of glacial valleys and joint orientations in the area.

537

538 The joints measured in this study are consistent with the steeply dipping, orthogonal joint sets measured in a nearby

539 structural survey in West Creek (Callahan and Wayland, 1965) and described in a geotechnical assessment of the rock slopes

540 above Skagway's cruise ship dock (Brennan and Whistler, 2022). High angle joints are likely formed by the tensile

541 component of shearing from the nearby Chatham Strait fault and Eastern Denali fault systems, while sheeting joints reflect

542 the combined influence of far field tectonic stresses and topographic stress that arise from landscape curvature (Martel, 2006,

543 2017). Rock slopes with orthogonal jointing are often predisposed to block toppling failure particularly where steep

544 orthogonal joints form the sides of toppling blocks and low angle joints, like the sheeting joints observed in this study, act as

545 the basal failure plane (Wyllie and Mah, 2004). Because the densest cluster of joints we observed dips steeply to the

546 southeast, rock slopes facing northwest tend to form anti-dip slopes which are conducive to toppling failure. This is

547 supported by larger and more abundant talus deposits on the east sides of the lower Skagway River valley and Nahku bay,

548 confirming that rockfall occurs preferentially on northwest-facing slopes (Fig. 6).

549

550 The results of our kinematic analysis demonstrate that rock slopes in the steep rugged terrain surrounding Skagway are more

551 susceptible to block toppling failure than planar slide failure. The preference for topping failure is due to the inclination of

552 joints, which are generally steep and conducive to toppling failure as their near verticality may preclude them from

553 daylighting in rock slope faces, a necessary condition for planar slide failure. On the west side of the lower Skagway River

554 valley, an isolated zone of steep vertical cliffs is susceptible to planar slide failure as recent planar failures are evident, which

555 release from sheeting joints and slide on joints steeply dipping southeast (Fig. 12).

556

557
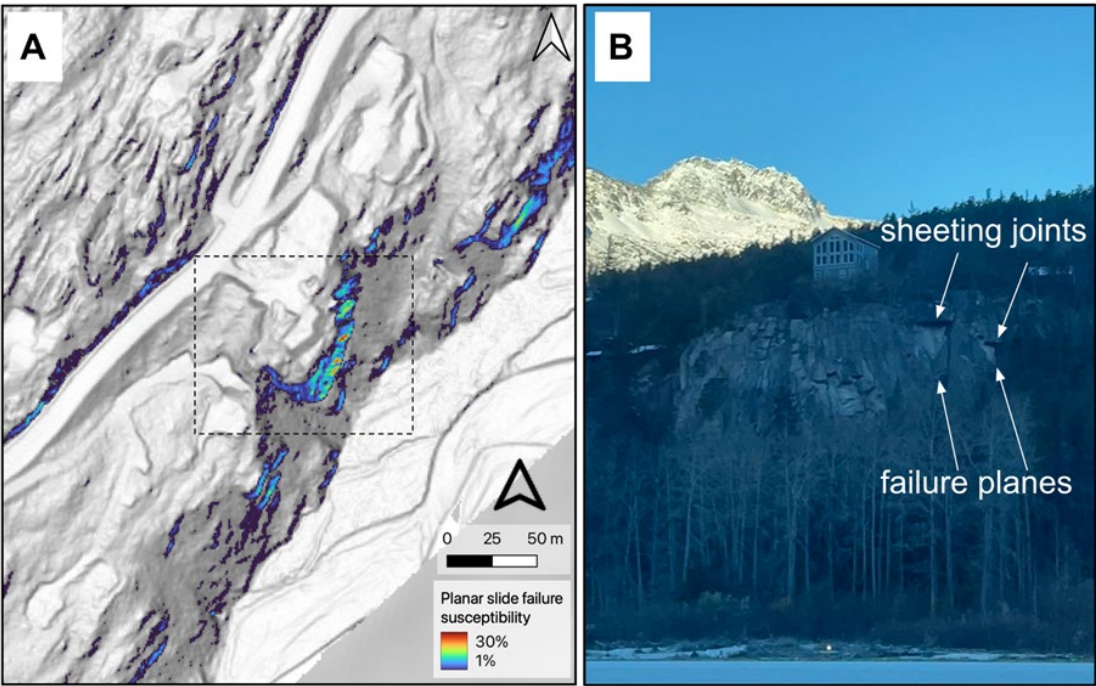
Figure 12: Planar sliding susceptibility along the western ridgeline in Skagway River Valley. Location depicted in Fig. 4. (a)
Map of planar failure susceptibility index using equation 1. (b) Image of SE-facing ridgeline in lower Skagway River valley.
Note high values on SE-facing steep bedrock cliffs that coincide with field evidence for sheeting joints and planar failures.
Hillshades derived from DGGS lidar data.

562

Rockfall susceptibility maps are consistent with the failure mode and location of rock slope deformation observed in the

field. Just uphill of the prominent escarpment along the eastern ridgeline in the lower Skagway River valley, we observed

numerous instances of detached parallel slabs of rock separated by tension cracks (Fig. 3). These blocks appear to be

experiencing early phases of toppling failure as vegetation and other processes contribute to crack widening. These

observations indicate that our predicted zones of toppling failure along active bedrock escarpments are likely to continue

propagating to the southeast providing additional blocks available to initiate rockfall. More generally, these observations

suggest that erosion and SE-oriented lateral migration of the eastern ridgeline has been substantial since the glacial retreat 10

to 12 kya. Reconstruction of the ridgeline to its immediate post-glacial geometry implies that 10 to 100 meters of lateral

erosion has occurred during the Holocene. On-going rockfall activity along this ridgeline suggests that this unravelling and

retreat of the escarpment will continue.

573

574 Importantly, extensive rockfall activity and lateral divide migration does not occur along the entire ridgeline. Rather, our

575 results show large sections of the 5-km long ridgeline with patchy and localized talus deposits and benchy bedrock

576 landforms. On Kinnse's Cliff (at 4 km on the railroad transect), for example, talus deposits extend upslope from the valley

577 floor to vertical cliff faces that terminate at the ridgeline (Fig. 5). In this area, rockfall susceptibility is relatively high, but

578 concentrated in a relatively small area of vertical rock slope, and a forested talus deposit and benchy zone sits between the

579 cliff and infrastructure in Skagway (Fig. 9). By contrast, several areas along the escarpment exhibit high potential for

580 rockfall runout to reach the valley. At the cruise ship dock (4.5 to 5 km), continuous, rockfall-prone slopes above the cruise

581 ship dock span from the escarpment to the base of the slope, resulting in a large area with high rockfall susceptibility in close

582 proximity to harbour infrastructure. Similarly, from 1.5 to 2.5 km on our railroad transect, a high-relief escarpment with

583 steep vertical bedrock outcrops near the crest exhibits a continuous steep slope to the valley floor (Fig. 10). In this area,

584 which is the source area for the Cemetery Slide, rockfall susceptibility and long runout potential are high and we observed

585 frequent spalling rocks during our field work (Fig. 10b). In addition, The Daily Alaskan reported a 1914 rockfall event just

586 south of the Cemetery Slide at 2.5km along the transect which coincides with our simulations of high rockfall runout

587 potential (Figs. 10 & 13). During that event, L. Gault noted "an avalanche of earth and stone" that "leaped the railroad

588 track…pounding against the fence." Gault noted that the railroad track served as a "safety barrier" because "the force of the

589 descent had been so much lessened." Further afield in the NE section of Nahku Bay, another zone of high rockfall

590 susceptibility is revealed by our analysis. Steep rocky slopes rise to an elevation of 250 m with close proximity to Dyea

591 Road. This area lacks a well-developed runout path, but it does coincide with source areas for two events in the AKDOT

592 rockfall inventory that impacted Dyea Road. Most generally, a rigorous characterization of rockfall risk in Skagway requires

593 estimation of occupation and usage of structures and transportation corridors coupled with our results (e.g., Michoud et al.,

594 2012).

595
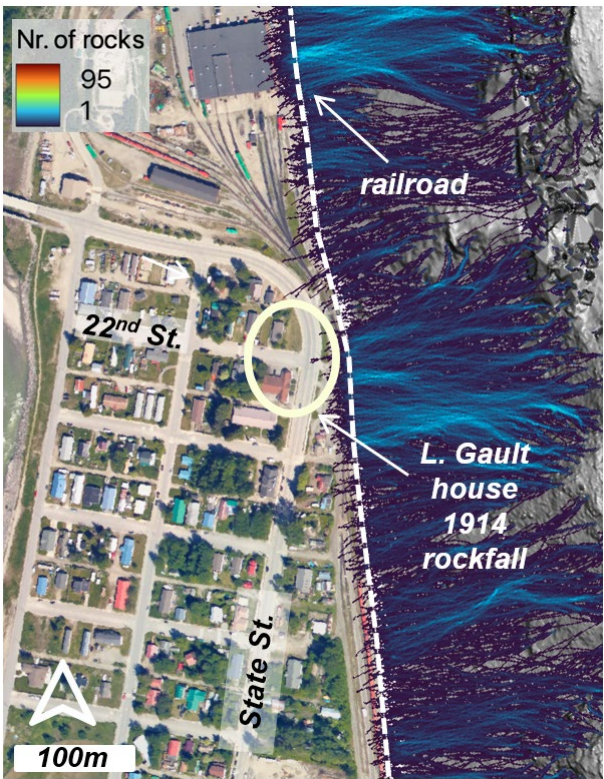
Figure 13: Detailed map of modeled rockfall runout (Medium rock (50th percentile), no forest) with location depicted shown by white box on Fig. 10b. Note the location of rockfall near the intersection of 22nd and State Street described by L. Gault in the March 26, 1914, edition of The Daily Alaskan. That location corresponds with a region of likely rockfall runout identified by our coupled initiation-runout simulations. Hillshade derived from DGGS lidar data. Background image from USGS NAIP (National Agriculture Imagery Program).

Our analyses reveal distinctive zones of high rockfall runout hazard in the Skagway region that result from the combination of glacial erosion that sets the morphology of bedrock slopes and the orientation of joint sets that determine the geometry of potential bedrock failures. Most likely, the orientation and extent of glacial erosion is not independent of the joints. Rather, we suspect that the nearly parallel orientation of joints and the N-NE trending ridgeline along the eastern margin of the lower Skagway River valley arise due to glacial erosion tracking discontinuities that facilitate erosion more readily than undeformed bedrock. Localized zones of the prominent ridgeline that abuts Skagway River valley exhibit abundant historic rockfall activity and over long timescales this activity is likely to continue. As such, our findings provide key constraints for identifying areas at risk to inform mitigation efforts.

6 Conclusions

Rock slope failure is a major driver of landscape evolution in Skagway since glacial retreat. The steeply dipping orthogonal joints in Skagway's rock slopes are conducive to block toppling failure. Our results highlight a distinct contrast in the morphology of Skagway River valley's eastern and western ridgelines, which is primarily determined by the predisposition of northwest-facing slopes to block toppling failure along a densely fractured joint set that dips steeply to the southeast. This is consistent with geomorphic evidence of extensive rockfall activity, where talus deposits are more abundant and larger on the eastern side of the lower Skagway River valley than the west. This structural control on rockfall activity is also reflected in the east and west sides of Nahku Bay, situated to the west of Skagway. Historic rockfall records indicate a similar preference for initiating on northwest-facing slopes. Our simulations show areas with high rockfall susceptibility that may merit further investigation and mitigation: 1) the ridgeline and slopes above the cruise ship dock, 2) the high-relief topography at the north end of Skagway (which includes the Cemetery Slide), and 3) the eastern ridgeline bordering Nahku Bay. Recent rockfall source areas located in these regions are characterized by steep northwest facing slopes that are highly susceptible to block toppling failure and reach >200 m in elevation which facilitates long runout paths.

7 Data availability

All topographic data used for analyses are cited within the text. The structural data are available as Supplemental material.

8 Author contribution

IW and JR conceived and designed the study and IW executed the study, RC provided on-site context, knowledge and guidance, AP contributed to study design and fieldwork, IW and JR prepared the manuscript with contributions from all other co-authors.

9 Acknowledgments

This research was funded by NSF Award #2052972 (Focused CoPe: Building Community Sensor Networks for Coastal Hazards and Climate Change Impacts in Southeast Alaska), which supports community-driven fundamental and translational geohazard science for project partners across SE Alaska. The authors thank leaders and members of the Skagway Traditional Council and residents of Skagway for their observations, critical insights, hospitality, and assistance; the Municipality of Skagway for sharing rockfall reports; and the NSF-funded UW RAPID facility for the timely acquisition of UAS lidar data. Conversations with Joe Wartman, Ben Leshchinsky, alex grant, Chris Massey, and Dimitrios Zekkos were insightful and contributed to our understanding of rockslope processes.

10 References

Abellán, A., Calvet, J., Vilaplana, J. M., and Blanchard, J.: Detection and spatial prediction of rockfalls by means of terrestrial laser scanner monitoring, Geomorphology, 119, 162–171, https://doi.org/10.1016/j.geomorph.2010.03.016, 2010.

Abellán, A., Vilaplana, J. M., Calvet, J., García-Sellés, D., and Asensio, E.: Rockfall monitoring by Terrestrial Laser Scanning – case study of the basaltic rock face at Castellfollit de la Roca (Catalonia, Spain), Natural Hazards and Earth System Sciences, 11, 829–841, https://doi.org/10.5194/nhess-11-829-2011, 2011.

Aksoy, H. and Ercanoglu, M.: Determination of the rockfall source in an urban settlement area by using a rule-based fuzzy evaluation, Natural Hazards and Earth System Sciences, 6, 941–954, https://doi.org/10.5194/nhess-6-941-2006, 2006.

Alejano, L. R., Veiga, M., Pérez-Rey, I., Castro-Filgueira, U., Arzúa, J., and Castro-Caicedo, Á. J.: Analysis of a complex slope failure in a granodiorite quarry bench, Bull Eng Geol Environ, 78, 1209–1224, https://doi.org/10.1007/s10064-017-1160-y, 2019.

Baichtal, J. F., Lesnek, A. J., Carlson, R. J., Schmuck, N. S., Smith, J. L., Landwehr, D. J., and Briner, J. P.: Late Pleistocene and early Holocene sea-level history and glacial retreat interpreted from shell-bearing marine deposits of southeastern Alaska, USA, Geosphere, 17, 1590–1615, https://doi.org/10.1130/GES02359.1, 2021.

Ballantyne, C. K.: A general model of paraglacial landscape response, The Holocene, 12, 371–376, https://doi.org/10.1191/0959683602hl553fa, 2002.

Barlow, J., Lim, M., Rosser, N., Petley, D., Brain, M., Norman, E., and Geer, M.: Modeling cliff erosion using negative power law scaling of rockfalls, Geomorphology, 139–140, 416–424, https://doi.org/10.1016/j.geomorph.2011.11.006, 2012.

Biegel, K. M., Gosselin, J. M., Dettmer, J., Colpron, M., Enkelmann, E., and Caine, J. S.: Earthquake Relocations Delineate a Discrete Fault Network and Deformation Corridor Throughout Southeast Alaska and Southwest Yukon, Tectonics, 43, e2023TC008140, https://doi.org/10.1029/2023TC008140, 2024.

Borella, J., Quigley, M., Krauss, Z., Lincoln, K., Attanayake, J., Stamp, L., Lanman, H., Levine, S., Hampton, S., and Gravley, D.: Geologic and geomorphic controls on rockfall hazard: how well do past rockfalls predict future distributions?, Natural Hazards and Earth System Sciences, 19, 2249–2280, https://doi.org/10.5194/nhess-19-2249-2019, 2019.

Bovis, M. J. and Evans, S. G.: Extensive deformations of rock slopes in southern Coast Mountains, southwest British Columbia, Canada, Engineering Geology, 44, 163–182, https://doi.org/10.1016/S0013-7952(96)00068-3, 1996.

Brennan, K. and Whistler, R.: Railroad dock landslide, initial site visit trip report, Skagway, Alaska, Geotechnical/Environmental Report, No. 109508-001, Shannon & Wilson, Anchorage, AK, USA, 2022.

Burns, W. J. and Madin, I. P.: Protocol for Inventory Mapping of Landslide Deposits from Light Detection and Ranging (lidar) Imagery, Oregon Department of Geology and Mineral Industries (DOGAMI) Special Paper 42, 36p., 2009.

Callahan and Wayland: Geologic reconnaissance of the West Creek damsite near Skagway, Alaska, Geological Survey Bulletin, 1211-A, https://doi.org/10.3133/b1211A, 1965.

Caviezel, A., Ringenbach, A., Demmel, S. E., Dinneen, C. E., Krebs, N., Bühler, Y., Christen, M., Meyrat, G., Stoffel, A., Hafner, E., Eberhard, L. A., Rickenbach, D. von, Simmler, K., Mayer, P., Niklaus, P. S., Birchler, T., Aebi, T., Cavigelli, L., Schaffner, M., Rickli, S., Schnetzler, C., Magno, M., Benini, L., and Bartelt, P.: The relevance of rock shape over mass— implications for rockfall hazard assessments, Nat Commun, 12, 5546, https://doi.org/10.1038/s41467-021-25794-y, 2021.

675   Choi, M., Eaton, D. W., and Enkelmann, E.: Is the Eastern Denali fault still active?, Geology, 49, 662–666,
676   https://doi.org/10.1130/G48461.1, 2021.

677   Collins, B. D. and Stock, G. M.: Rockfall triggering by cyclic thermal stressing of exfoliation fractures, Nature Geoscience, 9,
678   395–400, https://doi.org/10.1038/ngeo2686, 2016.

679   Corominas, J., van Westen, C., Frattini, P., Cascini, L., Malet, J.-P., Fotopoulou, S., Catani, F., Van Den Eeckhaut, M.,
680   Mavrouli, O., Agliardi, F., Pitilakis, K., Winter, M. G., Pastor, M., Ferlisi, S., Tofani, V., Hervás, J., and Smith, J. T.:
681   Recommendations for the quantitative analysis of landslide risk, Bull Eng Geol Environ, 73, 209–263,
682   https://doi.org/10.1007/s10064-013-0538-8, 2014.

683   Cruden, D. M.: Limits to common toppling, Can. Geotech. J., 26, 737–742, https://doi.org/10.1139/t89-085, 1989.

684   DGGS Staff: LiDAR Datasets of Alaska, Alaska Division of Geological & Geophysical Surveys,
685   https://doi.org/10.14509/25239, 2013.

686   Fanos, A. and Pradhan, B.: Laser Scanning Systems and Techniques in Rockfall Source Identification and Risk Assessment:
687   A Critical Review, Earth Systems and Environment, 2, https://doi.org/10.1007/s41748-018-0046-x, 2018.

688   Frattini, P., Crosta, G., Carrara, A., and Agliardi, F.: Assessment of rockfall susceptibility by integrating statistical and
689   physically-based approaches, Geomorphology, 94, 419–437, https://doi.org/10.1016/j.geomorph.2006.10.037, 2008.

690   Gigli, G., Lombardi, L., Carlà, T., Beni, T., and Casagli, N.: A method for full three-dimensional kinematic analysis of steep
691   rock walls based on high-resolution point cloud data, International Journal of Rock Mechanics and Mining Sciences, 157,
692   105178, https://doi.org/10.1016/j.ijrmms.2022.105178, 2022.

693   Grant, A., Wartman, J., and Abou-Jaoude, G.: Multimodal method for coseismic landslide hazard assessment, Engineering
694   Geology, 212, 146–160, https://doi.org/10.1016/j.enggeo.2016.08.005, 2016.

695   Guerriero, L., Annibali Corona, M., Di Martire, D., Francioni, M., Limongiello, M., Tufano, R., and Calcaterra, D.: Rockfall
696   susceptibility analysis of the "San Michele Arcangelo" historic trail (Central Italy) based on virtual outcrops and multiple
697   propagation models, Bull Eng Geol Environ, 83, 263, https://doi.org/10.1007/s10064-024-03764-0, 2024.

698   Guzzetti, F., Reichenbach, P., and Wieczorek, G. F.: Rockfall hazard and risk assessment in the Yosemite Valley, California,
699   USA, Natural Hazards and Earth System Sciences, 3, 491–503, https://doi.org/10.5194/nhess-3-491-2003, 2003.

700   Hales, T. C. and Roering, J. J.: Climatic controls on frost cracking and implications for the evolution of bedrock landscapes,
701   Journal of Geophysical Research, 112, https://doi.org/10.1029/2006JF000616, 2007.

702   Hungr, O., Evans, S. G., and Hazzard, J.: Magnitude and frequency of rock falls and rock slides along the main transportation
703   corridors of southwestern British Columbia, Can. Geotech. J., 36, 224–238, https://doi.org/10.1139/t98-106, 1999.

704   Hungr, O., Leroueil, S., and Picarelli, L.: The Varnes classification of landslide types, an update, Landslides, 11, 167–194,
705   https://doi.org/10.1007/s10346-013-0436-y, 2014.

706   Kundu, J., Sarkar, K., Ghaderpour, E., Mugnozza, G. S., and Mazzanti, P.: A GIS-Based Kinematic Analysis for Jointed Rock
707   Slope Stability: An Application to Himalayan Slopes, Land, 12, https://doi.org/10.3390/land12020402, 2023.

708   Leine, R. I., Schweizer, A., Christen, M., Glover, J., Bartelt, P., and Gerber, W.: Simulation of rockfall trajectories with
709   consideration of rock shape, Multibody Syst Dyn, 32, 241–271, https://doi.org/10.1007/s11044-013-9393-4, 2014.

Leith, K., Moore, J. R., Amann, F., and Loew, S.: In situ stress control on microcrack generation and macroscopic extensional fracture in exhuming bedrock: FRACTURE GENERATION IN EXHUMING BEDROCK, Journal of Geophysical Research: Solid Earth, 119, 594–615, https://doi.org/10.1002/2012JB009801, 2014.

Loye, A., Jaboyedoff, M., and Pedrazzini, A.: Identification of potential rockfall source areas at a regional scale using a DEM-based geomorphometric analysis, Nat. Hazards Earth Syst. Sci., 9, 1643–1653, https://doi.org/10.5194/nhess-9-1643-2009, 2009.

Lu, G., Caviezel, A., Christen, M., Demmel, S. E., Ringenbach, A., Bühler, Y., Dinneen, C. E., Gerber, W., and Bartelt, P.: Modelling rockfall impact with scarring in compactable soils, Landslides, 16, 2353–2367, https://doi.org/10.1007/s10346-019-01238-z, 2019.

Lu, G., Ringenbach, A., Caviezel, A., Sanchez, M., Christen, M., and Bartelt, P.: Mitigation effects of trees on rockfall hazards: does rock shape matter?, Landslides, 18, 59–77, https://doi.org/10.1007/s10346-020-01418-2, 2021.

Luckman, B. H.: Rockfalls and rockfall inventory data: Some observations from surprise valley, Jasper National Park, Canada, Earth Surface Processes, 1, 287–298, https://doi.org/10.1002/esp.3290010309, 1976.

Macpherson, A. E., Nicolsky, D. J., and Suleimani, E. N.: Digital elevation models of Skagway and Haines, Alaska: Procedures, data sources, and quality assessment, Alaska Division of Geological & Geophysical Surveys, https://doi.org/10.14509/29143, 2014.

Marquínez, J., Menéndez Duarte, R., Farias, P., and JiméNez Sánchez, M.: Predictive GIS-Based Model of Rockfall Activity in Mountain Cliffs, Natural Hazards, 30, 341–360, https://doi.org/10.1023/B:NHAZ.0000007170.21649.e1, 2003.

Martel, S. J.: Effect of topographic curvature on near-surface stresses and application to sheeting joints: EFFECT OF TOPOGRAPHIC CURVATURE, Geophysical Research Letters, 33, n/a-n/a, https://doi.org/10.1029/2005GL024710, 2006.

Martel, S. J.: Progress in understanding sheeting joints over the past two centuries, Journal of Structural Geology, 94, 68–86, https://doi.org/10.1016/j.jsg.2016.11.003, 2017.

Matasci, B., Stock, G. M., Jaboyedoff, M., Carrea, D., Collins, B. D., Guérin, A., Matasci, G., and Ravanel, L.: Assessing rockfall susceptibility in steep and overhanging slopes using three-dimensional analysis of failure mechanisms, Landslides, 15, 859–878, https://doi.org/10.1007/s10346-017-0911-y, 2018.

Matsuoka, N. and Sakai, H.: Rockfall activity from an alpine cliff during thawing periods, Geomorphology, 28, 309–328, https://doi.org/10.1016/S0169-555X(98)00116-0, 1999.

Menounos, B., Goehring, B. M., Osborn, G., Margold, M., Ward, B., Bond, J., Clarke, G. K. C., Clague, J. J., Lakeman, T., Koch, J., Caffee, M. W., Gosse, J., Stroeven, A. P., Seguinot, J., and Heyman, J.: Cordilleran Ice Sheet mass loss preceded climate reversals near the Pleistocene Termination, Science, 358, 781–784, https://doi.org/10.1126/science.aan3001, 2017.

Messenzehl, K., Meyer, H., Otto, J.-C., Hoffmann, T., and Dikau, R.: Regional-scale controls on the spatial activity of rockfalls (Turtmann Valley, Swiss Alps) — A multivariate modeling approach, Geomorphology, 287, 29–45, https://doi.org/10.1016/j.geomorph.2016.01.008, 2017.

Michoud, C., Derron, M.-H., Horton, P., Jaboyedoff, M., Baillifard, F.-J., Loye, A., Nicolet, P., Pedrazzini, A., and Queyrel, A.: Rockfall hazard and risk assessments along roads at a regional scale: example in Swiss Alps, Natural Hazards and Earth System Sciences, 12, 615–629, https://doi.org/10.5194/nhess-12-615-2012, 2012.

Moore, J. R., Sanders, J. W., Dietrich, W. E., and Glaser, S. D.: Influence of rock mass strength on the erosion rate of alpine cliffs, Earth Surface Processes and Landforms, 34, 1339–1352, https://doi.org/10.1002/esp.1821, 2009.

Moos, C., Khelidj, N., Guisan, A., Lischke, H., and Randin, C. F.: A quantitative assessment of rockfall influence on forest structure in the Swiss Alps, Eur J Forest Res, 140, 91–104, https://doi.org/10.1007/s10342-020-01317-0, 2021.

Munson, M.: Railroad Dock landslides continue, declaration of emergency in place, The Skagway News, 12th August, 2022a.

Munson, M.: Rockslide at cruise ship dock – Skagway's Railroad Dock has limited use, The Skagway News, 23rd June, 2022b.

Nash, D., Rutz, J. J., and Jacobs, A.: Atmospheric Rivers in Southeast Alaska: Meteorological Conditions Associated With Extreme Precipitation, Journal of Geophysical Research: Atmospheres, 129, e2023JD039294, https://doi.org/10.1029/2023JD039294, 2024.

Oliinyk, M., Bubniak, I., and Vikhot, Y.: Using Move software by geological field works, International Conference of Young Professionals «GeoTerrace-2020», 1–5, https://doi.org/10.3997/2214-4609.20205706, 2020.

Patton, A. I., Luna, L. V., Roering, J. J., Jacobs, A., Korup, O., and Mirus, B. B.: Landslide initiation thresholds in data-sparse regions: application to landslide early warning criteria in Sitka, Alaska, USA, Natural Hazards and Earth System Sciences, 23, 3261–3284, https://doi.org/10.5194/nhess-23-3261-2023, 2023.

Poage, N. J., Marshall, D. D., and McClellan, M. H.: Maximum Stand-Density Index of 40 Western Hemlock–Sitka Spruce Stands in Southeast Alaska, Western Journal of Applied Forestry, 22, 99–104, https://doi.org/10.1093/wjaf/22.2.99, 2007.

Priest, S. D. and Hudson, J. A.: Estimation of discontinuity spacing and trace length using scanline surveys, International Journal of Rock Mechanics and Mining Sciences & Geomechanics Abstracts, 18, 183–197, https://doi.org/10.1016/0148-9062(81)90973-6, 1981.

Rapp, A.: Talus slopes and mountain walls at Tempelfjorden, Spitsbergen : a geomorphological study of the denudation of slopes in an Arctic locality, Skritfter, Norsk Polarinstitutt, 119, 1960.

Roering, J. J., Dedinsky, K., Grilliot, M., Wachino, I. D., and Cash, R.: Skagway Landslide Hazard, RAPID Facility, https://doi.org/doi.org/10.17603/ds2-2e3p-yn12, 2025.

Rosser, N. and Massey, C.: Rockfall hazard and risk, in: Landslide Hazards, Risks, and Disasters, Elsevier, 581–622, https://doi.org/10.1016/B978-0-12-818464-6.00013-5, 2022.

Rosser, N., Lim, M., Petley, D., Dunning, S., and Allison, R.: Patterns of precursory rockfall prior to slope failure, Journal of Geophysical Research: Earth Surface, 112, https://doi.org/10.1029/2006JF000642, 2007.

Royán, M. J., Abellán, A., Jaboyedoff, M., Vilaplana, J. M., and Calvet, J.: Spatio-temporal analysis of rockfall pre-failure deformation using Terrestrial LiDAR, Landslides, 11, 697–709, https://doi.org/10.1007/s10346-013-0442-0, 2014.

Samodra, G., Chen, G., Sartohadi, J., Hadmoko, D. S., Kasama, K., and Setiawan, M. A.: Rockfall susceptibility zoning based on back analysis of rockfall deposit inventory in Gunung Kelir, Java, Landslides, 13, 805–819, https://doi.org/10.1007/s10346-016-0713-7, 2016.

Sarro, R., Rossi, M., Reichenbach, P., and Mateos, R. M.: From rockfall source areas identification to susceptibility zonation: a proposed workflow tested in El Hierro (Canary Islands, Spain), Natural Hazards and Earth System Sciences Discussions, 1–30, https://doi.org/10.5194/nhess-2024-85, 2024.

Stock, G. M. and Collins, B. D.: Quantitative Rockfall hazard and risk assessment for Yosemite Valley, Yosemite National Park, California, USGS Scientific Investigations Report 2014-5129, 2014.

Stock, G. M., Bawden, G. W., Green, J. K., Hanson, E., Downing, G., Collins, B. D., Bond, S., and Leslar, M.: High-resolution three-dimensional imaging and analysis of rock falls in Yosemite Valley, California, Geosphere, 7, 573–581, https://doi.org/10.1130/GES00617.1, 2011.

Terzaghi, R. D.: Sources of Error in Joint Surveys, Géotechnique, 15, 287–304, https://doi.org/10.1680/geot.1965.15.3.287, 1965.

The Daily Alaskan: SLIDE: Hill again caves in near Moore's Wharf, The Daily Alaskan, 20th October, 1, 1901.

Thompson, P.: Alaska Department of Transportation & Public Facilities (AKDOT) Geotechnical Asset Management Program, Technical Report STP000S(802)(B), Juneau, AK, 2017.

Thornton, T. F.: Our Grandparents' Names on the Land/Haa Leelk'w Has Aani Saax'u, University of Washington Press, Seattle, WA, 256 pp., 2010.

Utlu, M., Öztürk, M. Z., Şimşek, M., and Akgümüş, M. F.: Evaluation of rockfall hazard based on UAV technology and 3D Rockfall Simulations, International Journal of Environment and Geoinformatics, 10, 1–16, https://doi.org/doi.10.30897/ijegeo.10323768, 2023.

Whalley, B.: Rockfalls, in: Slope Instability, Wiley, Chichester, UK, 217–256, 1984.

Wieczorek, G. F. and Jäger, S.: Triggering mechanisms and depositional rates of postglacial slope-movement processes in the Yosemite Valley, California, Geomorphology, 15, 17–31, https://doi.org/10.1016/0169-555X(95)00112-I, 1996.

Wright, B. E., Plumb, P., Wright, J., and Biles, F. E.: Historical photographs from U.S. Forest Service research and development activities in Alaska, https://doi.org/10.2737/RDS-2021-0084, 2021.

Wyllie, D. C. and Mah, C. W.: Rock Slope Engineering, 4th ed., Spon, 456 pp., 2004.

Yehle, L. A. and Lemke, R. W.: Reconnaissance engineering geology of the Skagway area, Alaska with emphasis on evaluation of earthquake and other geologic hazards, USGS Open File Report, 1972.